
This is the **accepted version** of the journal article:

Sanna, Daniele; Ugone, Valeria; Sciortino, Giuseppe; [et al.]. «VIVO complexes with antibacterial quinolone ligands and their interaction with serum proteins». Dalton transactions, Vol. 47, Issue 7 (February 2018), p. 2164-2182. DOI 10.1039/c7dt04216g

This version is available at <https://ddd.uab.cat/record/288754>

under the terms of the  **IN** COPYRIGHT license

Complexes of $V^{IV}O^{2+}$ ion with antibacterial quinolone ligands and their interaction with serum proteins

Daniele Sanna,^{*a} Valeria Ugone,^b Giuseppe Sciortino,^{b,c} Péter Buglyó,^d Zsolt Bihari,^d
Péter László Parajdi-Losonczai,^d Eugenio Garribba,^{*b}

^a *Istituto CNR di Chimica Biomolecolare, Trav. La Crucca 3, I-07040 Sassari, Italy. E-mail: daniele.sanna@icb.cnr.it; Tel: +39 079 2841207.*

^b *Dipartimento di Chimica e Farmacia, Università di Sassari, Via Vienna 2, I-07100 Sassari, Italy. E-mail: garribba@uniss.it; Tel: +39 079 229487.*

^c *Departament de Química, Universitat Autònoma de Barcelona, 08193 Cerdanyola del Vallès, Barcelona, Spain*

^d *Department of Inorganic and Analytical Chemistry, University of Debrecen, H-4032 Debrecen, Egyetem tér 1, Hungary*

* Corresponding authors.

† Electronic Supplementary Information (ESI) available: ^{51}V hyperfine coupling constants calculated for $V^{IV}O$ species of the model ligand L^Q (Table S1), structure of the model ligand L^Q , and mono- and bis-chelated $V^{IV}O$ complexes (Schemes S1-S3), experimental and simulated isotopic pattern for ESI-MS spectrum recorded in the system $V^{IV}O^{2+}$ /nalidixic acid (Figure S1), anisotropic EPR spectra recorded in the systems $V^{IV}O^{2+}$ /levofloxacin (Figures S2-S4), $V^{IV}O^{2+}$ /ciprofloxacin (Figure S5), and $V^{IV}O^{2+}$ /levofloxacin/1-methylimidazole and $V^{IV}O^{2+}$ /sparfloxacin/1-methylimidazole (Figure S6).

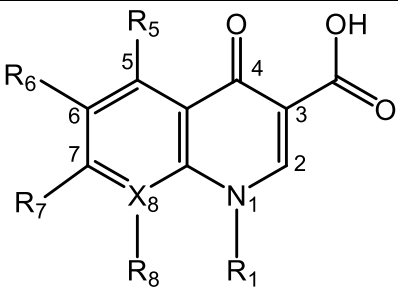

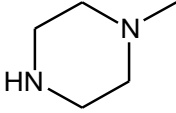
Abstract

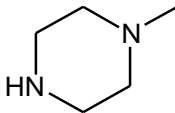
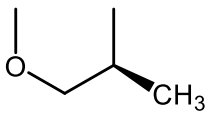
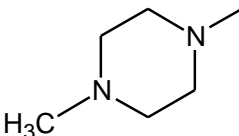

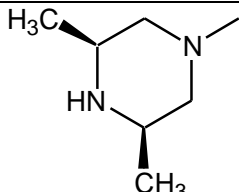
Quinolone derivatives are among the most commonly prescribed antibacterials in the world and could also have interest as organic ligands in the design of metal complexes with potential pharmacological activity. In this study five compounds, belonging to the first (nalidixic acid or Hnal), second (ciprofloxacin or Hcip, and norfloxacin or Hnor) and third generation (levofloxacin or Hlev, and sparfloxacin or Hspar) of quinolones, were used as ligands to bind $V^{IV}O^{2+}$ ion. In aqueous solution mono- and bis-chelated species were formed as a function of pH, with *cis*- $[VOH_xL_2(H_2O)]^{x+}$ and $[VOH_xL_2]^{x+}$, $x = 0-2$, being the major complexes at pH 7.4. DFT calculations indicate that the most stable isomers are the octahedral *OC*-6-32 and *OC*-6-34, and the square pyramidal *SPY*-5-12, in equilibrium with each other. To the best of our knowledge, this is the first case that an equilibrium between a penta-coordinated square pyramidal and a hexa-coordinated octahedral complex is observed in solution for ligands forming six-membered chelated rings. Nalidixic acid forms the solid compound $[VO(nal)_2(H_2O)]$, to which a *cis*-octahedral geometry was assigned. The interaction with 1-methylimidazole (MeIm) causes a shift of the equilibrium SPY -5 + $H_2O \rightleftharpoons OC$ -6 toward right after the formation of *cis*- $[VOH_xL_2(MeIm)]^{x+}$, where MeIm replaces an equatorial water ligand. The study of the systems containing $[VO(nal)_2(H_2O)]$ and the serum proteins – albumin (HSA), apo-transferrin (apo-hTf) and holo-transferrin (holo-hTf) – indicates that HSA and holo-hTf form the mixed species $\{VO(nal)_2\}_y(HSA)$ and $\{VO(nal)_2\}_y(holo-hTf)$, where $y = 1-3$ denotes the number of $VO(nal)_2$ moieties bound to accessible histidines (His105, His367, His510 for HSA, and His25, His349, His606 for holo-hTf), whereas apo-hTf yields $VO(nal)_2(apo-hTf)$ with the coordination of the His289 residue only. Docking calculations suggest that the specific conformation of apo-hTf and the steric repulsion of the moiety *cis*- $VO(nal)_2$ hinder its interaction with all the surface His residues and the formation of a hydrogen bond network which could stabilize the binding sites.

1. Introduction

The family of 4-quinolone compounds (or simply quinolones) includes some of the most commonly prescribed antibacterials in the world,^{1, 2, 3, 4, 5, 6} which are active against a wide variety of Gram-negative and Gram-positive bacterial infections. Many diseases are today treated with quinolones, including urinary tract infections, sexually transmitted diseases, prostatitis, skin and tissue infections, chronic bronchitis, and intra-abdominal and pelvic infections,⁷ even if an increasing resistance has been observed in all the types of bacteria. In addition, quinolones are used in the treatment of tuberculosis, which causes the death of more than one million people every year.⁸

The first member of quinolone drugs was nalidixic acid, isolated in 1960s,⁹ used for the treatment of uncomplicated urinary tract infections caused by enteric bacteria.² In 1970s other molecules belonging to the first-generation of quinolones, such as oxolinic acid and cinoxacin, were introduced into the clinic.^{10, 11} However, their application has been limited by their narrow spectrum of activity.⁵ For this reason, in 1980s several changes on the structure were proposed and the second-generation of compounds was developed, based on the introduction of a heterocycle in position 7 of the quinolone structure, as piperazine, methylpiperazine or pyrrolidine, and a F atom in position 6 (Scheme 1).^{1, 2, 3, 4, 5, 6} Among these compounds, named fluoroquinolones,¹² norfloxacin, ciprofloxacin, and ofloxacin are worth of being mentioned. They show improved pharmacokinetics and pharmacodynamics and are more active than nalidixic acid against Gram-positive bacteria. Ciprofloxacin was the first quinolone molecule which showed a high activity outside of the urinary tract.^{1, 2, 5, 6}

								
Name	Gener.	Abbr.	X ₈	R ₁	R ₈	R ₅	R ₆	R ₇
Nalidixic acid	First	Hnal	N	C ₂ H ₅	–	H	H	CH ₃
Ciprofloxacin	Second	Hcip	C		H	H	F	

Norfloxacin	Second	Hnor	C	C ₂ H ₅	H	H	F	
Levofloxacin	Third	Hlev	C		H	F		
Sparfloxacin	Third	Hspar	C	F		NH ₂	F	

Scheme 1. Name, generation, abbreviation and structure of the quinolone ligands studied in this work.

The subsequent generation of quinolones, the third-generation, is characterized by substitutions at positions 7 and 8 and displays a wide spectrum of activity, in particular against Gram-positive species, and include levofloxacin, moxifloxacin, and sparfloxacin.^{1, 2, 3, 4, 5, 6}

Metal complexes of quinolones have been reported in the literature.^{13, 14} Initially, the formation of metal species was considered a negative phenomenon affecting the efficiency of quinolones and the reduction of their antimicrobial activity in the presence of metal ions supported this assumption;¹⁵ several mechanisms, among which the chelation of carboxylate and keto groups and the formation of insoluble complexes in the gastrointestinal tract, were proposed to explain the decrease of the bioavailability of quinolones in the presence of metal ions.^{16, 17} Nevertheless, from the pharmacological point of view, the quinolone–metal ion interaction suggests a potential synergistic effect of the metal on the antimicrobial activity. For many metal complexes an equal or higher activity than the parent free quinolone has been observed, since the chelation increases the lipophilicity of the central metal ion and makes easier the transport through the lipid membranes and the uptake by cells. Inside the nucleus the metal favours the interaction between quinolone and DNA through an intercalative binding.¹⁸ Over the last years, also the antifungal activity, not exhibited by quinolones, and anticancer activity have been examined: *in vitro* biological results have shown that the Cu^{II}–quinolone complexes could be a valuable tool in the cancer chemotherapy.¹⁸

Vanadium compounds show a wide variety of pharmacological properties.^{19, 20} One of the most important applications of V derivatives in medicine is the potential use in the therapy of patients suffering from type 2 diabetes mellitus.²¹ Several neutral V^{IV}O species formed by bidentate anionic

organic ligands L^- with composition $[V^{IV}OL_2]$ and coordination $VO(O_4)$ ²² and $VO(N_2O_2)$ ²³ have been proposed. Among them, $[VO(\text{maltolato})_2]$ or BMOV is the benchmark compound for the new molecules with anti-diabetic action.²⁴ Other potential pharmacologically active V complexes include spermicidal, anti-HIV, antiparasitic, antiviral, antituberculosis and antitumor drugs.^{19, 25} Therefore, it appears to be interesting to combine the antibiotic activity of quinolones with those displayed by V. This approach based on the combination of the pharmacological activity of on organic ligand with that of a metal ion (particularly, V^{IV}) has been followed by Etcheverry and co-workers in a number of papers.²⁶ The advantages to use quinolones with respect to the other possible organic ligands are as follows: they are non-toxic, have overcome all the clinical tests for their use in medicine and easily penetrate the body membranes such as cell and nucleus membranes. Furthermore quinolones, as demonstrated in the literature, can form stable V species at the physiological pH,²⁷ and this could ensure to the complexes the optimal lipophilicity to cross the biological membranes.

The stability of the compounds $[V^{IV}OL_2]$ largely influences the pharmacological efficacy by determining the absorption in the gastrointestinal tract, the transport in the blood, the uptake by the target cells, and overall the availability of the actual anti-diabetic species.²⁸ Depending on the geometry assumed in aqueous solution at the physiological pH and thermodynamic stability of $[VOL_2]$, the interaction with the blood and intracellular proteins can occur.²⁹ Such an interaction seems to play a key role in the transport and mechanism of action of pharmacologically active V compounds and has been investigated by our³⁰ and other groups.³¹ Therefore, the complete knowledge of the complexation scheme, thermodynamic stability of the formed species, and their interaction with the proteins are factors fundamental to understand which could be the active species in the organism.³²

For these reasons, in this work the interaction of $V^{IV}O^{2+}$ with five quinolone ligands belonging to first-, second- and third-generation (Scheme 1) was studied in the solid state and aqueous solution. To evaluate the possible binding with His residues, the ternary systems $V^{IV}O^{2+}$ /quinolone/1-methylimidazole were also examined at the physiological pH. Finally, the systems formed by the bis-chelated $V^{IV}O$ species and two serum proteins, transferrin and albumin, were examined. The study was carried out through the combined application of instrumental (pH-potentiometry, Electron Paramagnetic Resonance or EPR, and Electrospray Ionization Mass Spectrometry or ESI-MS) and computational methods (Density Functional Theory or DFT and docking calculations). These techniques provide valuable information on the coordination mode of the organic ligands and proteins to $V^{IV}O^{2+}$ ion.^{33, 34, 35}

The overall results of this study could provide insights into the possible experimentation of $V^{IV}O$ -quinolone complexes as potential metal based drugs.

2. Experimental and Computational Section

2.1. Chemicals

The organic ligands nalidixic acid (1-ethyl-1,4-dihydro-7-methyl-4-oxo-1,8-naphthyridine-3-carboxylic acid, Hnal; code N8878), ciprofloxacin (1-cyclopropyl-6-fluoro-4-oxo-7-(piperazin-1-yl)-1,4-dihydroquinoline-3-carboxylic acid, Hcip; PHR1167), norfloxacin (1-ethyl-6-fluoro-1,4-dihydro-4-oxo-7-(1-piperazinyl)-3-quinoline-carboxylic acid, Hnor; N9890), levofloxacin ((S)-9-fluoro-3-methyl-7-oxo-10-(4-methyl-1-piperazinyl)-2,3-dihydro-7H-pyrido[1,2,3-de][1,4]-benzoxazine-6-carboxylic acid, Hlev; 28266), sparfloxacin (5-amino-1-cyclohexyl-7-(*cis*-3,5-dimethylpiperazino)-6,8-difluoro-1,4-dihydro-4-oxo-3-quinolinecarboxylic acid, Hspar; 56968), 1-methylimidazole (MeIm; M50834) and (4-(2-hydroxyethyl)piperazine-1-ethanesulfonic acid (HEPES; H3375) are all Sigma-Aldrich products and were used without further purification.

Human serum apo-transferrin (apo-hTf; T4283), human serum holo-transferrin (holo-hTf; T4132) and human serum albumin (HSA; A1887) were purchased from Sigma-Aldrich with molecular mass of 76-81 kDa, 76-81 kDa and 66 kDa, respectively.

$V^{IV}O^{2+}$ solutions were prepared from $VOSO_4 \cdot 3H_2O$ (oxidovanadium(IV) sulfate trihydrate; 204862), produced by Sigma-Aldrich, following literature methods.³⁶

2.2. Synthesis of $[VO(nal)_2(H_2O)] \cdot 2H_2O$

The complex $[VO(nal)_2(H_2O)] \cdot 2H_2O$ was synthesized according to the procedure established in the literature for quinolone derivatives.³⁷ A methanolic solution (15 mL) of nalidixic acid (0.400 mmol, 92.9 mg), deprotonated with KOH (0.400 mmol, 22.5 mg), was added to a methanolic solution (10 mL) of $VOSO_4 \cdot 3H_2O$ (0.200 mmol, 43.4 mg) and the reaction mixture was refluxed for 2 h. The green precipitate was filtered off and dried. Anal. Calc. (%) for $[VO(nal)_2(H_2O)] \cdot 2H_2O$, $C_{24}H_{28}N_4O_{10}V$ (583.44): C, 49.41, H, 4.84, N, 9.60; found: C, 49.85; H, 4.51; N, 9.51. IR: (ν_{max}/cm^{-1}): $\nu(O-H)$, 3410(m); $\nu_{as}(COO)$, 1636(vs); $\nu(C=O)_{ket}$, 1605(vs); $\nu_{as}(COO)$, 1384(s); $\nu(V=O)$, 972(s).

2.3. Preparation of the solutions for EPR measurements

The solutions were prepared dissolving in ultrapure water, obtained through the purification system Millipore MilliQ Academic, or in a mixture H₂O/DMSO 50/50 (w/w), a weighted amount of VOSO₄·3H₂O and the ligands to obtain a metal ion concentration of 1.0×10^{-3} M and a metal to ligand molar ratio of 1:2. Argon was bubbled through the solutions to ensure the absence of oxygen and avoid the oxidation of V^{IV}O²⁺ ion.

In the experiments with apo-hTf and holo-hTf, the pH of the solutions containing V^{IV}O²⁺ and Hnal was raised to *ca.* 4.0 and NaHCO₃ and HEPES were added in appropriate amounts in order to have concentration of 2.5×10^{-2} and 1.0×10^{-1} M, respectively. Subsequently, pH was brought to *ca.* 6.5, apo-hTf or holo-hTf were added, pH was increased up to 7.4 and EPR spectra were immediately measured. The final ratio V^{IV}O²⁺/Hnal/apo-hTf or V^{IV}O²⁺/Hnal/holo-hTf was 2:4:1 with a protein concentration of 5.0×10^{-4} M. In the experiments with HSA a procedure analogous to that established in the literature was used, with the difference that NaHCO₃ was not added.[30a](#), [30b](#) The final ratio V^{IV}O²⁺/Hnal/HSA was 4:8:1 with a protein concentration of 2.5×10^{-4} M.

2.4. Preparation of the solutions for ESI-MS measurements

The solution containing [VO(nal)₂(H₂O)] was prepared dissolving the solid complex in DMSO (1.0×10^{-2} M) and an aliquot was diluted to 5.0×10^{-6} M with ultrapure water (LC-MS grade, Sigma-Aldrich). After the preparation of the solution, ESI-MS spectra were recorded immediately.

2.5. Spectroscopic and analytical measurements

EPR spectra were recorded at 120 or 298 K with an X-band (9.4 GHz) Bruker EMX spectrometer equipped with an HP 53150A microwave frequency counter. When the signal to noise ratio was low due to the V^{IV}O²⁺ concentration, signal averaging was used.[38](#) In the sections 3.2 and 3.3, the values of the ⁵¹V hyperfine coupling constants along the *z* axis (*A_z*) were compared with those estimated on the basis of the “additivity rule”, which relates *A_z* to the number and type of the equatorial ligands, assigning them a specific contribution. This empirical rule has been proved and accepted in a large number of papers.[39](#) Usually, the experimental values of *A_z* fall in the range of $\pm 3 \times 10^{-4}$ cm⁻¹ with

respect to those estimated with the “additivity rule”.³⁹ The contributions of the keto-O, carboxylate-O⁻, His-N and H₂O were taken from refs. ^{39b, 39c}.

Mass spectra in positive- and negative-ion mode were obtained on a Q Exactive™ Plus Hybrid Quadrupole-Orbitrap™ (Thermo Fisher Scientific) mass spectrometer. The solutions were infused at a flow rate of 5.00 μ L/min into the ESI chamber immediately after their preparation. The spectra were recorded in the m/z range 50-750 at a resolution of 140,000 and accumulated for at least 5 min in order to increase the signal-to-noise ratio. The experimental conditions used for the measurements were: spray voltage 2300 V, capillary temperature 250 °C, sheath gas 5-10 (arbitrary units), auxiliary gas 3 (arbitrary units), sweep gas 0 (arbitrary units), probe heater temperature 50 °C (positive mode); spray voltage -1900 V, capillary temperature 250 °C, sheath gas 20 (arbitrary units), auxiliary gas 5 (arbitrary units), sweep gas 0 (arbitrary units), probe heater temperature 14 °C (negative mode). The spectra were analysed by using Thermo Xcalibur 3.0.63 software (Thermo Fisher Scientific).

Infrared (IR) spectra (4000-600 cm^{-1}) were recorded with a JASCO FT/IR-480Plus spectrometer using KBr disks.

Elemental analysis (C, H, N) was carried out with a Perkin-Elmer 240 B elemental analyzer.

2.6. Potentiometric measurements

Levofloxacin and its $\text{V}^{\text{IV}}\text{O}^{2+}$ complexes were studied in aqueous solution, while the pH-potentiometric measurements for nalidixic acid and its $\text{V}^{\text{IV}}\text{O}^{2+}$ complexes were carried out in DMSO/H₂O 70/30 (w/w) mixture due to the limited water solubility. In all the cases an ionic strength of 0.20 M (KCl) and temperature of 25.0 ± 0.1 °C were used. Carbonate-free KOH solution of known concentration (*ca.* 0.20 M) in water or in the above solvent mixture was employed as titrant. HCl stock solutions were prepared from concentrated HCl in water or in the DMSO/H₂O mixture and their concentrations were determined by potentiometric titrations. A Mettler Toledo titrator equipped with a combined glass electrode (type 6.0234.100) was used. IUPAC recommendations were employed to carry out the measurements in DMSO/H₂O 70/30 (w/w) solvent mixture: the electrode was conditioned for three days in the solvent mixture prior the measurements.⁴⁰ The electrode system was calibrated according to the procedures suggested by Irving et al.⁴¹ The water ionization constant, $\text{p}K_{\text{w}}$, was found to be 13.76 ± 0.01 in aqueous medium, while it is 17.13 ± 0.01 in the DMSO/H₂O mixture, in excellent agreement with literature data.⁴² The titrations were performed in the pH range 2.0-11.0 in water, 2.0-14.0 in the solvent mixture or until precipitation occurred. Initial volume of the samples was 15.00 mL. The ligand concentration

was varied in the range 0.001-0.003 M and the metal ion to ligand ratios in the range 1:1-1:4. Typically, three or four ratios were measured in each system. Reproducibility of the titration points included in the evaluation was within 0.005 pH units. Titration points with a waiting time of 10 min or more were omitted from the calculations. The accepted fitting of the titration curves was always less than 0.006 mL. The samples were in all the cases completely deoxygenated by bubbling purified argon for *ca.* 20 min prior measurements and also during the titrations. The stability of the complexes, reported as the logarithm of the overall formation constant $\beta_{\text{pqr}} = [\text{VO}_p\text{L}_q\text{H}_r]/[\text{VO}]_p[\text{L}]_q[\text{H}]_r$ where VO stands for the metal ion, L for the deprotonated form of the ligand and H is the proton, has been calculated with the aid of the PSEQUAD program.⁴³ The uncertainties (3σ values) of the stability constants are given in parentheses. During the calculations the following hydroxido complexes of $\text{V}^{\text{IV}}\text{O}^{2+}$ were assumed: $[\text{VO}(\text{OH})]^+$ ($\log\beta_{10-1} = -5.94$), $[(\text{VO})_2(\text{OH})_2]^{2+}$ ($\log\beta_{20-2} = -6.95$), with stability constants taken from Henry et al.,⁴⁴ and corrected for the different ionic strengths by use of the Davies equation,⁴⁵ $[\text{VO}(\text{OH})_3]^-$ ($\log\beta_{10-3} = -18.0$) and $[(\text{VO})_2(\text{OH})_5]^-$ ($\log\beta_{20-5} = -22.0$).^{46, 47}

2.7. DFT Calculations

All the calculations presented in this paper were performed with DFT methods using the software Gaussian 09 (revision C.01).⁴⁸

The geometry and harmonic frequencies of the $\text{V}^{\text{IV}}\text{O}$ complexes were optimized at B3P86/6-311g level of theory with the procedure reported in the literature.⁴⁹ This choice ensures a good degree of accuracy in the prediction of the structures of first-row transition metal complexes⁵⁰ and, in particular, of vanadium compounds.⁴⁹ Mono- and bis-chelated $\text{V}^{\text{IV}}\text{O}$ species formed by nalidixic acid and 1-methyl-4-oxo-1,4-dihydroquinoline-3-carboxylate (chosen as a model for all the other quinolone derivatives and indicated generically with L^{Q} , Scheme S1 of ESI) were examined and the structures simulated were ($\text{L} = \text{nal}$ or L^{Q}): $[\text{VO}(\text{L})(\text{H}_2\text{O})_2]^+$, $[\text{VO}(\text{L})(\text{H}_2\text{O})_3]^+$, $[\text{VO}(\text{L})_2]$, *trans*- $[\text{VO}(\text{L})_2(\text{H}_2\text{O})]$ and *cis*- $[\text{VO}(\text{L})_2(\text{H}_2\text{O})]$. Concerning the square pyramidal and *trans*-octahedral complexes only two options exist (*SPY*-5-12 and *SPY*-5-13, and *OC*-6-42 and *OC*-6-43), whereas for *cis*-octahedral species four isomers are possible (*OC*-6-23, *OC*-6-24, *OC*-6-32 and *OC*-6-34).⁵¹ The possible structures of the mono- and bis-chelated complexes are represented in Schemes S2 and S3 of ESI.

On the optimized structures, the ^{51}V hyperfine coupling constants (A) were calculated using the half-and-half hybrid functional BHandHLYP and the basis set 6-311+g(d), according to the procedures previously published.⁵² It must be taken into account that for a $\text{V}^{\text{IV}}\text{O}^{2+}$ species A_z is

usually negative, but in the literature its absolute value is often reported; this formalism was also used in a number of points of this study. The theory background was described in detail in ref. [53](#). The percent deviation (PD) of the absolute calculated value, $|A_z|^{\text{calcd}}$, from the absolute experimental value, $|A_z|^{\text{exptl}}$, was obtained as follows: $100 \times [(|A_z|^{\text{calcd}} - |A_z|^{\text{exptl}})/|A_z|^{\text{exptl}}]$.

The relative stability of the square pyramidal (*SPY*-5-12 and *SPY*-5-13) and *cis*-octahedral (*OC*-6-23, *OC*-6-24, *OC*-6-32 and *OC*-6-34) complexes formed by nalidixic acid was calculated at the B3P86/6-311g level of theory computing the solvent effect (in this study, water) using the continuum SMD model,[54](#) which gives good results in the prediction of solvation Gibbs energy.[54](#) The total value of the Gibbs energy in aqueous solution ($G^{\text{tot}}_{\text{aq}}$) for each species can be separated into the electronic plus nuclear repulsion energy (E^{ele}), the thermal contribution (G^{therm}) and the solvation energy (ΔG^{solv}): $G^{\text{tot}}_{\text{aq}} = E^{\text{ele}} + G^{\text{therm}} + \Delta G^{\text{solv}}$. The Gibbs energy in the gas phase ($G^{\text{tot}}_{\text{gas}}$) can be found by neglecting the term ΔG^{solv} : $G^{\text{tot}}_{\text{gas}} = E^{\text{ele}} + G^{\text{therm}}$. The thermal contribution was estimated using the ideal gas model and the calculated harmonic vibrational frequencies to determine the correction due to the zero point energy and to the thermal population of the vibrational levels.[55](#)

2.8. Docking calculations

Docking calculations were performed with GOLD 5.2 software[56](#) on the X-ray structures available in the Protein Data Bank (PDB) of HSA (PDB code: 1ao6[57](#)), apo-transferrin (PDB: 2hau[58](#)) and holo-transferrin (PDB: 3v83[59](#)). All crystallographic water and small molecules included in the PDB files were removed and the hydrogen atoms added with the UCSF Chimera program.[60](#)

The simulations were carried out constructing an evaluation sphere with a radius of 12 Å centred, for each docking, in the region of interest. The protein side chains flexibility was taken into account using the Dunbrack rotamers libraries[61](#) implemented in GOLD software. Genetic algorithm (GA) parameters have been set using 50 GA runs and a minimum of 100,000 operations. The rest of GA parameters, including pressure, number of islands, niche size, crossover, mutation and migration were set to default.

The scoring (*Fitness* of GoldScore) was evaluated applying the modified version of GoldScore scoring function, which was validated in a recent study.[62](#) The scoring associated with each pose related to the (V complex)–protein interaction is reported in eq. 1:

$$\text{Fitness } (F) = \alpha \cdot S_{\text{hbond}}^{\text{ext}} + \beta \cdot S_{\text{vdW}}^{\text{ext}} + \gamma \cdot S_{\text{hbond}}^{\text{int}} + \delta \cdot (S_{\text{vdW}}^{\text{int}} - S_{\text{tors}}) \quad (1)$$

where S_{hbond}^{ext} and S_{vdW}^{ext} are the scoring terms due to the hydrogen bonds (*hbond*) and van der Waals (*vdW*) intermolecular interactions, S_{hbond}^{int} and S_{vdW}^{int} represent the intramolecular interactions, S_{tors} evaluates the change in stability due to the molecular torsions, and α , β , γ , and δ are empirical parameters optimized to weigh the different interactions.

To identify the possible regions of interaction between the bis-chelated V^{IV}O complexes formed by nalidixic acid and the proteins, relative Solvent Excluded Surface (SES)⁶³ calculations were preliminarily performed focusing on the most exposed histidine residues.

The docking calculations were carried out as follows. Briefly, the selected energy minima of *cis*-[VO(nal)₂(H₂O)], optimized with the method described in the section 2.7, were preliminary treated removing the H₂O ligand from the fourth equatorial coordination site and adding a dummy hydrogen atom according to the procedure established recently.⁶⁴ All dockings were computed considering the possible dihedral changes along the aliphatic bonds applying the GOLD algorithm. The solutions were analyzed by means of GaudiView.⁶⁵

The best solutions of the calculations were evaluated through two main criteria: (a) the scoring (*Fitness* of GoldScore) associated with each pose, as reported in eq. 1 and (b) the population of the clusters containing the best structure.

The second coordination sphere interaction analysis was carried out with NCIPlot (Non-Covalent Interactions Plot).⁶⁶ This method bases its predictions computing the reduced gradient of the electron density (*s*) versus the electron density (ρ) multiplied by the sign of the second Hessian eigenvalue (λ_2). Strong stabilizing interactions (e.g. H-bond type) typically corresponds to values of $\rho > 0.01$ a.u. and $\lambda_2 < 0$. Strong destabilizing interactions (e.g. steric crowding) are associated to values of $\rho > 0.01$ a.u. and $\lambda_2 > 0$. For delocalized weak interactions (e.g. van der Waals) both density and gradient are small (typically $\rho < 0.01$ a.u.), and consequently $\lambda_2 \sim 0$.

3. Results and discussion

3.1. Ligands

The behaviour of two quinolone ligands was studied by pH-potentiometric methods: nalidixic acid (Hnal) and levofloxacin (Hlev) (Table 1). Whereas the systems containing levofloxacin and V^{IV}O²⁺/levofloxacin were studied in water, those with nalidixic acid – poorly soluble in water – were titrated in a mixture H₂O/DMSO 30/70 (w/w). The stability constants of the V^{IV}O²⁺ complexes

are summarized in Table 1. The data for ciprofloxacin (Hcip) have been already reported in the literature.^{27, 67}

Except for nalidixic acid, quinolones have two titratable protons, those on the carboxylic group and secondary amino group of the piperazine ring. In the literature, the values in the range 5.33-6.53 (pK_{a1}) were attributed to the carboxylic group, while those between 7.57 and 9.33 (pK_{a2}) to the piperazinium nitrogen.⁶⁸

The results obtained in this study confirm the previous data: in water the lower pK_a (pK_{a1} of 6.06 for H_2lev^+ and 6.17 for H_2cip^+) can be assigned to the deprotonation of $COOH$, whereas the higher pK_a (pK_{a2} of 8.18 for $Hlev$ and 8.54 for $Hcip$) is due to the deprotonation of the piperazine- NH^+ . As pointed out in the literature,²⁷ the high value of pK_{a1} for the carboxylic group can be explained with the formation of an intramolecular hydrogen bond between the $COOH$ and CO functionalities, which results in the formation of a six-membered ring.

Nalidixic acid has only one pK_a belonging to the carboxylic group. Its value measured in DMSO/ H_2O 70/30 (w/w) is 7.85, significantly higher than those determined in water for levofloxacin and ciprofloxacin (6.06 and 6.17, Table 1), and for nalidixic acid itself (5.94-6.13⁶⁹). This difference can be explained considering two points: i) the experimental pH readings in the mixture DMSO/ H_2O are larger than in water because of the different dielectric constant of the two systems;⁷⁰ ii) in the solvent mixture the neutral form of the ligand is stabilized and, for this reason, the loss of a proton is shifted to higher pH, resulting in the increase of the pK_a value compared to that in water.

Table 1. Stepwise deprotonation constants (pK_a) of the quinolone ligands and stability constants ($\log\beta$) of the binary $V^{IV}O^{2+}$ complexes at 25.0 ± 0.1 °C and $I = 0.20$ M (KCl).^a

	Nalidixic acid ^b	Levofloxacin ^c	Ciprofloxacin ^{c,d}
pK_{a1}	7.85(5)	6.06(1)	6.17
pK_{a2}	–	8.18(1)	8.54
$[VO(HL)]^{2+}$	–	14.79(2)	15.11
$[VOL]^+$	8.41(3)	9.74(5)	
$[VO(HL)_2]^{2+}$	–	29.12(1)	30.64
$[VO(HL)(L)]^+$	–	21.92(3)	24.4
$[VOL_2]$	14.41(14)	13.99(7)	
$[VOL(OH)]$	–	2.0(5)	

Fitting parameter ^c	0.00560	0.00578	0.00606
Number of fitted data points	139	335	92
pH range	2.0-7.5	2.0-11.0	2.0-7.0

^a The standard deviations are given between parentheses. ^b H₂O/DMSO 30/70 (w/w). ^c H₂O. ^d Ref. [27](#). ^e Fitting parameter is the average difference between the calculated and experimental titration curves expressed in mL of the titrant.

3.2. $V^{IV}O^{2+}$ /nalidixic acid (Hnal) system

The stability constants of the system $V^{IV}O^{2+}$ /Hnal were measured in a mixture DMSO/H₂O 70/30 (w/w) (Table 1). The distribution diagram of the species formed as a function of pH with a metal to ligand molar ratio of 1:2 is shown in Figure 1. The formation of complexes with composition $[VOL]^+$ and $[VOL_2]$ is observed, with the bis-chelated complex being the major species at physiological pH. The hydrolysis starts at pH higher than 8 with the formation of $[(VO)_2(OH)_5]^-$ and $[VO(OH)_3]^-$.

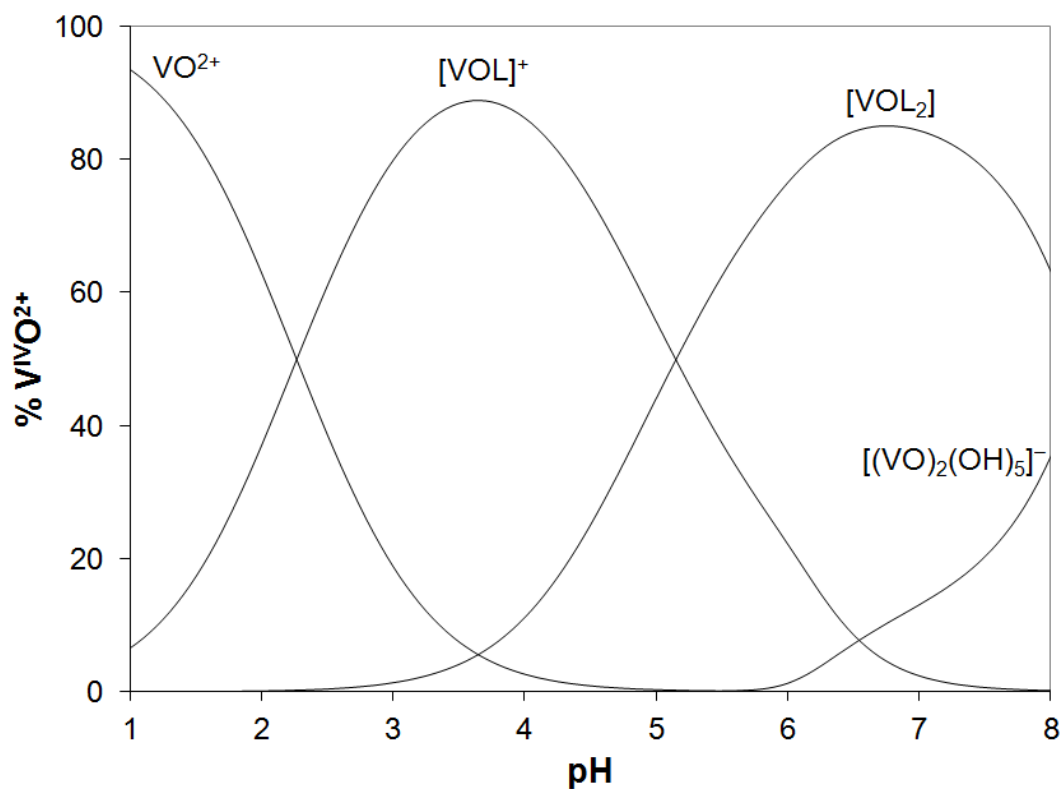


Figure 1. Distribution diagram as a function of pH of the species formed in the system $V^{IV}O^{2+}/Hnal$ (HL) with a total $V^{IV}O^{2+}$ concentration of 1.0×10^{-3} M and metal to ligand molar ratio of 1:2.

EPR spectra recorded on the system $V^{IV}O^{2+}/Hnal$ 1:2 in a mixture DMSO/H₂O 50/50 (w/w) confirmed the presence in solution of the mono-chelated and bis-chelated $V^{IV}O$ complexes under these experimental conditions (Figure 2). The values of g_z and A_z for $[VOL]^+$ (**I** in Figure 2) are 1.941 and $175.4 \times 10^{-4} \text{ cm}^{-1}$; the value of A_z estimated (A_z^{estmtd}) with the “additivity rule” [39a](#), [39b](#) for an equatorial coordination mode (CO, COO⁻; H₂O; H₂O) is $176.8 \times 10^{-4} \text{ cm}^{-1}$, in good agreement with that experimentally observed. At higher pH, in the range 5-9, the signals of two different species in equilibrium (**II** and **III** in Figure 2) appear: the spin Hamiltonian parameters are $g_z = 1.940$ and $A_z = 174.6 \times 10^{-4} \text{ cm}^{-1}$ for **II** and $g_z = 1.946$ and $A_z = 168.1 \times 10^{-4} \text{ cm}^{-1}$ for **III**. These signals were assigned to the hexa-coordinated *cis*-octahedral (**II**) and penta-coordinated square pyramidal complexes (**III**) and the application of the “additivity rule” allowed us to confirm this attribution; in fact, A_z^{estmtd} for the two possible equatorial coordination modes of **II**, (CO, COO⁻; CO; H₂O) and (CO, COO⁻; COO⁻; H₂O), is in the range $(173.3\text{-}174.7) \times 10^{-4} \text{ cm}^{-1}$ and for the equatorial coordination (CO, COO⁻; CO, COO⁻) of **III** is $171.2 \times 10^{-4} \text{ cm}^{-1}$. To the best of our knowledge, this is the first equilibrium between a square pyramidal and a *cis*-octahedral complex observed in solution for ligands forming six-membered chelated rings; all the previous cases reported in the literature concerned species with five-membered rings.[30e](#), [71](#), [72](#) Such a behaviour can explain the interaction of this family of compounds with the proteins because the equilibrium $[VOL_2] + H_2O \rightleftharpoons cis-[VOL_2(H_2O)]$ is shifted toward right upon the replacement of the equatorial water molecule by an amino acid residue.[30a](#), [30b](#) Other examples of equilibria between five- and six-coordinate geometries were reported for vanadium(V) complexes studied as models for the V–protein binding.[73](#)

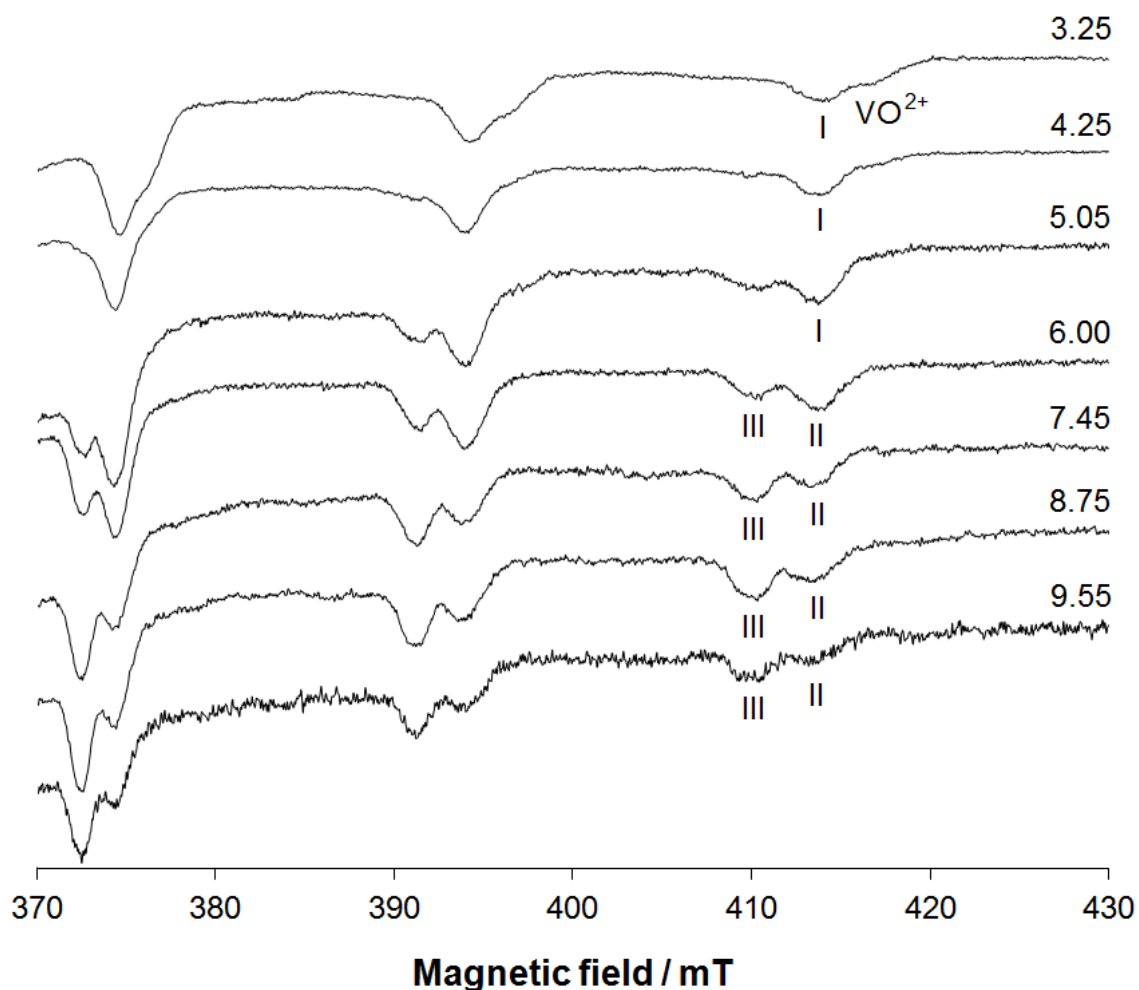


Figure 2. High field region of the X-band anisotropic EPR spectra recorded in a mixture H₂O/DMSO 50/50 (w/w) at 120 K as a function of pH in the system V^{IV}O²⁺/Hnal with a molar ratio of 1:2 and V concentration of 1.0×10^{-3} M. With V^{IV}O²⁺, **I**, **II** and **III** are indicated the $M_I = 7/2$ resonances of the species [VO(H₂O)₅]²⁺, [VO(nal)(H₂O)₃]⁺, *cis*-[VO(nal)₂(H₂O)] (*OC*-6-32 or *OC*-6-34) and [VO(nal)₂] (*SPY*-5-12), respectively.

The results of pH-potentiometry and EPR spectroscopy were confirmed by ESI-MS technique, which has been demonstrated over the last years very useful for the characterization of systems containing V.⁷⁴ The mass spectrum recorded in positive mode shows two peaks at $m/z = 233.09$ and $m/z = 255.07$, attributable to the protonated form of the ligand [Hnal+H]⁺ and the sodium adduct [Hnal+Na]⁺. At $m/z = 454.04$ the peak of [V^{IV}O(nal)(DMSO)₂]⁺ is observed, while those at $m/z = 530.10$ and $m/z = 552.08$ are assigned to the adducts formed by [V^{IV}O(nal)₂] with H⁺ and Na⁺, respectively. The comparison between the experimental and calculated isotopic pattern attributable to [V^{IV}O(nal)₂+H]⁺ ion is shown as an example in Figure 3; in particular, the peaks due to the natural abundance of ¹³C isotope (separated by $m/z \sim 1.00$ for this adduct with charge +1) allowed

us to confirm the assignment proposed above. These results demonstrate the presence in solution, under the experimental conditions examined in this study, of the mono- and bis-chelated $V^{IV}O$ species. Unfortunately, it was not possible to reveal the water molecule in the equatorial position of $V^{IV}O^{2+}$ ion, but this is in line with the literature data which suggest that a monodentate solvent molecule can be removed from the first metal coordination sphere during the ionization process.⁷⁵

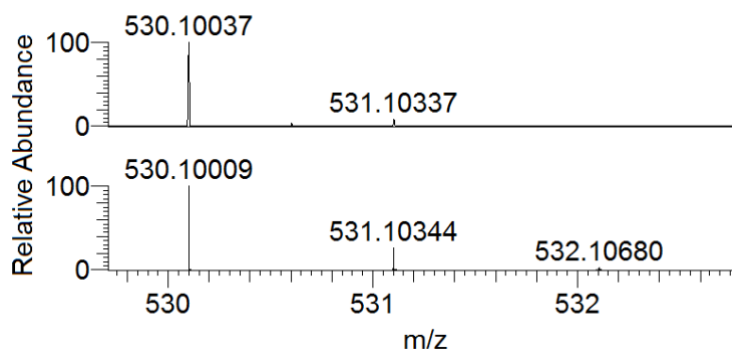
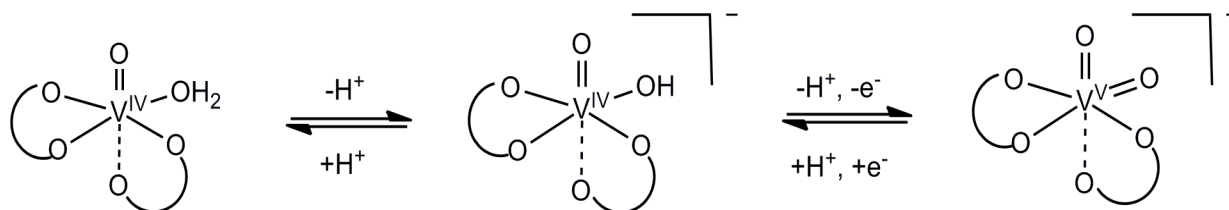


Figure 3. Experimental (above) and calculated (below) isotopic pattern for the peak of $[V^{IV}O(nal)_2+H]^+$ revealed at $m/z = 530.10$ in the positive ESI-MS spectrum recorded on the system $V^{IV}O^{2+}/Hnal$ 1:2 (ultrapure LC-MS water, V concentration 5.0×10^{-6} M).

The ESI-MS spectrum recorded in the negative-mode shows the presence in solution of the bis-chelated species with a deprotonated water molecule, $[V^{IV}O(nal)_2(OH)]^-$, and the related species of V^V , $[V^VO_2(nal)_2]^-$, at m/z 546.10 and 545.09, respectively (Figure S1 of ESI). It can be noticed that, since their mass differ by $m/z \sim 1$, the molecular peak M of the V^{IV} complex (at $m/z = 546.10$) and the M+1 peak of the isotopic pattern of V^V species (at $m/z = 546.09$, due to the presence of ^{13}C isotope) are superimposed. The detection of $[V^VO_2(nal)_2]^-$ can be explained with the formation of *cis*- $[V^{IV}O(nal)_2(H_2O)]$ in aqueous solution and can be due to two (partial) oxidation processes, the first in solution and the second one in-source during the recording of the spectrum.⁷⁶ The oxidation is probably favoured by the structure of the *cis*- $V^{IV}O(H_2O)^{2+}$ moiety, which gives the *cis*- $V^VO_2^+$ ion without any structural rearrangement (Scheme 2). The same behaviour was recently observed for the potential antitumor drug *cis*- $[V^{IV}O(Me_2phen)_2(H_2O)]^{2+}$, where Me_2phen is 4,7-dimethyl-1,10-phenanthroline, which gives *cis*- $[V^VO_2(Me_2phen)_2]^+$ when studied by ESI-MS spectrometry.⁷⁷

Finally, the peak at $m/z = 231.08$ observed in the negative ESI-MS spectrum is attributed to the deprotonated form of the ligand, $[nal]^-$. All the ions revealed in the spectra are listed in Table 2.

From the comparison between the experimental and calculated values, it can be noticed that the relative errors are always smaller than 2.0 ppm.



Scheme 2. Oxidation of *cis*-[V^{IV}O(nal)₂(H₂O)] to give *cis*-[V^VO₂(nal)₂]⁻.

Table 2. Species identified with ESI-MS spectrometry in the system V^{IV}O²⁺/Hnal 1:2.

Ion	Composition	Exptl m/z ^a	Calcd m/z ^a	Error (ppm) ^b
[Hnal+H] ⁺	C ₁₂ H ₁₃ N ₂ O ₃	233.09225	233.09207	0.8
[Hnal+Na] ⁺	C ₁₂ H ₁₂ N ₂ NaO ₃	255.07406	255.07401	0.2
[nal] ⁻	C ₁₂ H ₁₁ N ₂ O ₃	231.07734	231.07752	-0.8
[V ^{IV} O(nal)(DMSO) ₂] ⁺	C ₁₆ H ₂₃ N ₂ O ₆ S ₂ V	454.04314	454.04317	-0.1
[V ^{IV} O(nal) ₂ +H] ⁺	C ₂₄ H ₂₃ N ₄ O ₇ V	530.10037	530.10009	0.5
[V ^{IV} O(nal) ₂ +Na] ⁺	C ₂₄ H ₂₂ N ₄ NaO ₇ V	552.08192	552.08203	-0.2
[V ^{IV} O(nal) ₂ (OH)] ⁻	C ₂₄ H ₂₃ N ₄ O ₈ V	546.09684	546.09610	1.4
[V ^V O ₂ (nal) ₂] ⁻	C ₂₄ H ₂₂ N ₄ O ₈ V	545.08892	545.08828	1.2

^a The experimental and calculated m/z values refer to the monoisotopic representative peak. ^b Deviation in ppm from the calculated values, calculated as $10^6 \times [(\text{Exptl m/z} - \text{Calcd m/z})/\text{Calcd m/z}]$.

Since DFT calculations are very helpful in assigning the coordination modes of the metal species, the geometry of the V^{IV}O complexes formed by nalidixic acid was optimized using Gaussian 09 software (as described in the section 2.7). In addition, DFT methods were used to predict the value of the ⁵¹V hyperfine coupling constants (*A*^{calcd}) for the species observed in aqueous solution with EPR spectroscopy using the functional BHandHLYP and a triple- ζ basis set; these conditions allow calculating *A_z* for V^{IV}O species formed by ligands with N or O donors with a mean percent

deviation (MDP) below 1% and a mean absolute percent deviation (MADP) below 3% from the experimental A_z (A_z^{exptl}).^{53b}

The calculated components of the tensor A and the comparison with A_z^{exptl} are reported in Table 3. DFT methods suggest that mono-chelated complex (**I** in Figure 2) is octahedral with two water molecules in the equatorial plane and one water axially bound in *trans* to V=O group (Scheme S2 of ESI). This appears to be coherent with the data in the literature; for example, the mono-chelated $V^{IV}O$ complex formed by a similar (O, O) ligand, such as oxalate, is octahedral with three water molecules coordinated to V (two in the equatorial and one in the axial position).⁷⁸

Table 3. ^{51}V A values calculated at the level of theory BHandHLYP/6-311+g(d) with Gaussian 09 software for the $V^{IV}O$ species formed by nalidixic acid.^a

Complex ^b	Isomer	A_x^{calcd}	A_y^{calcd}	A_z^{calcd}	A_z^{exptl}	PD ^c
$[\text{VO}(\text{nal})(\text{H}_2\text{O})_2]^+$	–	-75.6	-78.6	-181.5	-175.4	3.5
$[\text{VO}(\text{nal})(\text{H}_2\text{O})_3]^+$	–	-72.2	-73.9	-176.2	-175.4	0.5
<i>cis</i> - $[\text{VO}(\text{nal})_2(\text{H}_2\text{O})]$	OC-6-23	-62.2	-66.9	-168.2	-174.6	-3.7
<i>cis</i> - $[\text{VO}(\text{nal})_2(\text{H}_2\text{O})]$	OC-6-24	-66.2	-69.7	-170.3	-174.6	-2.5
<i>cis</i>-$[\text{VO}(\text{nal})_2(\text{H}_2\text{O})]$	OC-6-32	-70.8	-71.5	-173.6	-174.6	-0.6
<i>cis</i>-$[\text{VO}(\text{nal})_2(\text{H}_2\text{O})]$	OC-6-34	-70.3	-72.1	-173.3	-174.6	-0.7
$[\text{VO}(\text{nal})_2]$	SPY-5-12	-61.1	-66.5	-169.5	-168.1	0.8
$[\text{VO}(\text{nal})_2]$	SPY-5-13	-58.3	-64.0	-167.0	-168.1	-0.7
<i>trans</i> - $[\text{VO}(\text{nal})_2(\text{H}_2\text{O})]$	OC-6-42	-55.3	-62.6	-161.7	-168.1	-3.8
<i>trans</i> - $[\text{VO}(\text{nal})_2(\text{H}_2\text{O})]$	OC-6-43	-51.0	-59.6	-157.3	-168.1	-6.4
<i>cis</i>-$[\text{VO}(\text{nal})_2(\text{1-MeIm})]$	OC-6-32	-61.7	-63.2	-163.4	-169.1	-3.4
<i>cis</i>-$[\text{VO}(\text{nal})_2(\text{1-MeIm})]$	OC-6-34	-61.4	-64.2	-163.7	-169.1	-3.2

^a All the A values are reported in 10^{-4} cm^{-1} . ^b In bold the species probably formed in aqueous solution are indicated. ^c Percent deviation (PD) with respect to the absolute experimental value calculated as: $100 \times [(|A_z|^{\text{calcd}} - |A_z|^{\text{exptl}})/|A_z|^{\text{exptl}}]$.

Concerning the isomers of the bis-chelated species, A_z calculated for square pyramidal $[\text{VO}(\text{nal})_2]$ species (**III** in Figure 2) is $-169.5 \times 10^{-4} \text{ cm}^{-1}$ for SPY-5-12 and $-167.0 \times 10^{-4} \text{ cm}^{-1}$ for SPY-5-13, equidistant from $-168.1 \times 10^{-4} \text{ cm}^{-1}$ experimental (PD of 0.8 and -0.7%, respectively). The values

of A_z^{calcd} for *trans*-octahedral species with a water in *trans* to V=O are significantly smaller ($-161.7 \times 10^{-4} \text{ cm}^{-1}$ for OC-6-42 and $-157.3 \times 10^{-4} \text{ cm}^{-1}$ for OC-6-43, very far from A_z^{exptl} of $-168.1 \times 10^{-4} \text{ cm}^{-1}$) and not compatible with the experimental ones; therefore, the weak coordination of a water molecule in the axial site, which would lower the experimental value of A_z , can be ruled out.⁷⁹

The value of A_z^{calcd} for *cis*-octahedral species (**II** in Figure 2) is as follows: for OC-6-23 it is $-168.2 \times 10^{-4} \text{ cm}^{-1}$, for OC-6-24 $-170.3 \times 10^{-4} \text{ cm}^{-1}$, for OC-6-32 $-173.6 \times 10^{-4} \text{ cm}^{-1}$ and for OC-6-34 $-173.3 \times 10^{-4} \text{ cm}^{-1}$, to be compared with A_z^{exptl} of $-174.6 \times 10^{-4} \text{ cm}^{-1}$. These data would suggest that in solution OC-6-32 and OC-6-34 isomers (with two equatorial CO, Scheme S3 of ESI) are slightly more stable than OC-6-23 and OC-6-24 (with two COO⁻ in the equatorial plane, Scheme S3).

To understand which bis-chelated species is the most stable in aqueous solution, the calculation of the Gibbs energy for the reactions $SPY-5-12 \rightleftharpoons SPY-5-13$ and $SPY-5-12 + \text{H}_2\text{O} \rightleftharpoons OC-6-(23,24,32,34)$ was performed (see section 2.7). For the reactions involving the *cis*-octahedral species the contribution of the water molecule was included in the calculations. The results are reported in Table 4.

Table 4. ΔG values of formation (in the gas phase and aqueous solution) and solvation for the formation of *cis*-octahedral and SPY-5-13 V^{IV}O isomer from SPY-5-12 formed by nalidixic acid.^{a,b}

Reaction	Temp. / K	$\Delta G^{\text{tot}}_{\text{gas}}$	$\Delta(\Delta G^{\text{solv}})$	$\Delta G^{\text{tot}}_{\text{aq}}$
$SPY-5-12 \rightleftharpoons SPY-5-13$	298	28.4	-23.9	4.5
$SPY-5-12 + \text{H}_2\text{O} \rightleftharpoons OC-6-32$	298	-7.9	49.4	41.5
$SPY-5-12 + \text{H}_2\text{O} \rightleftharpoons OC-6-34$	298	-6.0	52.6	46.6
$SPY-5-12 + \text{H}_2\text{O} \rightleftharpoons OC-6-24$	298	-7.9	56.2	48.3
$SPY-5-12 + \text{H}_2\text{O} \rightleftharpoons OC-6-23$	298	16.5	35.8	52.3
$SPY-5-12 \rightleftharpoons SPY-5-13$	120	28.9	-23.9	5.0
$SPY-5-12 + \text{H}_2\text{O} \rightleftharpoons OC-6-32$	120	-33.6	49.4	15.8
$SPY-5-12 + \text{H}_2\text{O} \rightleftharpoons OC-6-34$	120	-31.4	52.6	21.2
$SPY-5-12 + \text{H}_2\text{O} \rightleftharpoons OC-6-24$	120	-33.6	56.2	22.6
$SPY-5-12 + \text{H}_2\text{O} \rightleftharpoons OC-6-23$	120	-8.9	35.8	26.9

^a Values reported in kJ mol⁻¹. ^b Calculations performed at the B3P86/6-311g level of theory using SMD model for water.

It can be noted that the most stable species is *SPY*-5-12 with *SPY*-5-13 slightly higher in Gibbs energy; the optimized structures of these isomers are represented in Figure 4, a and b. This would suggest that the two species could be in equilibrium under the experimental conditions used, with $\Delta G^{\text{tot}}_{\text{gas}}$ favouring *SPY*-5-12 and $\Delta(\Delta G^{\text{solv}})$ favouring *SPY*-5-13. DFT prediction of A_z (Table 3) does not help us to demonstrate if only one or both these isomers are formed in aqueous solution. The structure expected for *SPY*-5-13 should be characterized by a negligible trigonal bipyramidal distortion with a value of the trigonality index τ of 0.007 ($\tau = (\beta - \alpha)/60$, with β and α being the pseudo-axial and pseudo-equatorial angles, is 1 for a regular trigonal bipyramid and 0 for a regular square pyramid ⁸⁰). In contrast, for *SPY*-5-12 – in which two short ($\text{V}-\text{O}_{\text{carb}} = 1.933 \text{ \AA}$) and two long bonds ($\text{V}-\text{O}_{\text{ket}} = 2.016 \text{ \AA}$) are in *trans* position – a much higher value of τ is predicted (0.386), in agreement with the data reported in the literature for similar compounds.⁸¹

The Gibbs energy for the reaction $\text{SPY-5} + \text{H}_2\text{O} \rightleftharpoons \text{OC-6}$ is significantly higher than that for the equilibrium $\text{SPY-5-12} \rightleftharpoons \text{SPY-5-13}$, mainly for the unfavourable value of $\Delta(\Delta G^{\text{solv}})$. Among the *cis*-octahedral isomers, *OC*-6-32 and *OC*-6-34 (Figure 4, c and d) with two equatorial O_{ket} are more stable than *OC*-6-23 and *OC*-6-24 both at 298 and 120 K (the temperature at which anisotropic EPR spectra were recorded), even if the differences are small. This confirms the above discussion based on the calculation of A_z , which indicates that the values predicted for *OC*-6-32 and *OC*-6-34 are closer to the experimental ones than those for *OC*-6-23 and *OC*-6-24.

In Table 5 the selected structural data for the square pyramidal and *cis*-octahedral isomers are listed, while in Tables S2-S7 of ESI are shown their optimized Cartesian coordinates.

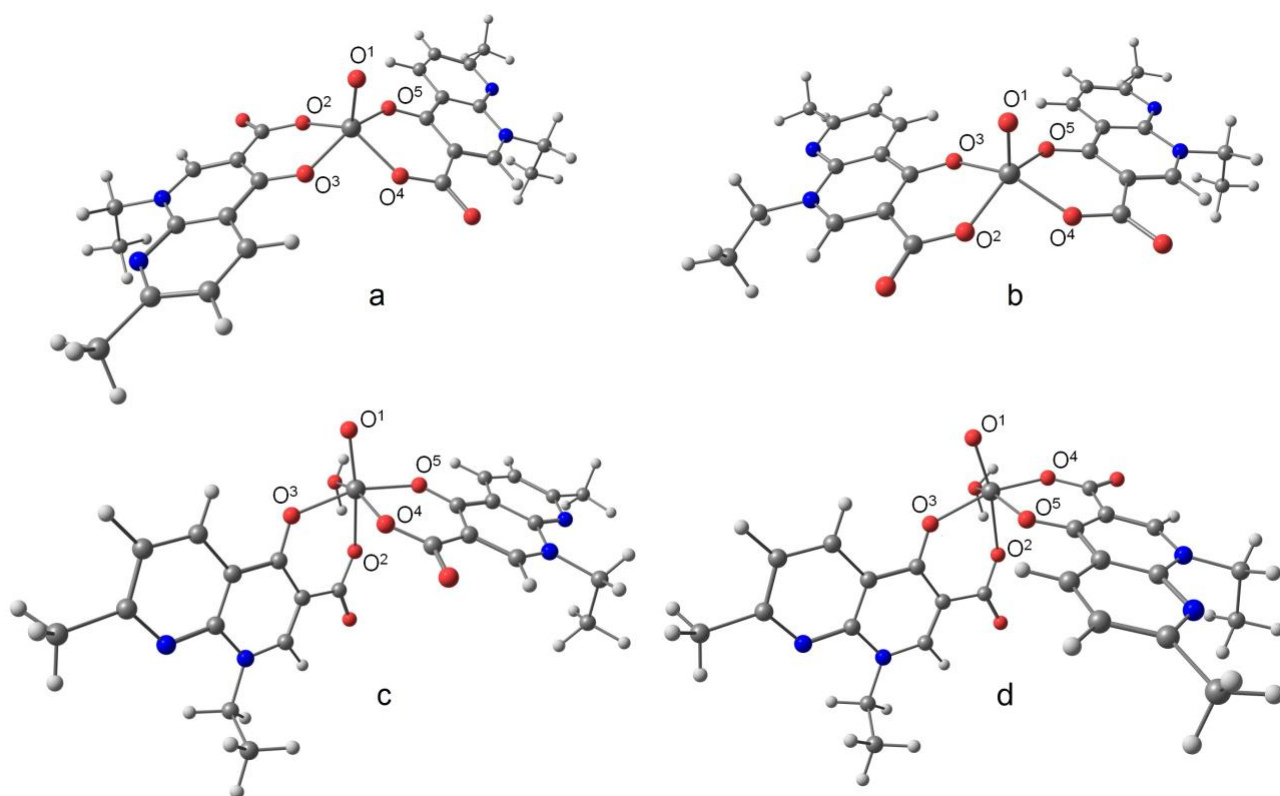


Figure 4. Optimized structures of the isomers *SPY-5-12* (a), *SPY-5-13* (b), *OC-6-32* (c) and *OC-6-34*, formed by nalidixic acid.

Table 5. Selected bond lengths and angles predicted by DFT methods for the isomers *SPY-5-12*, *SPY-5-13*, *OC-6-32* and *OC-6-34* formed by nalidixic acid.^a

Parameter ^{b,c}	<i>SPY-5-12</i>	<i>SPY-5-13</i>	<i>OC-6-32</i>	<i>OC-6-34</i>
V–O ¹	1.585	1.584	1.596	1.592
V–O ²	1.933	1.939	2.152	2.161
V–O ³	2.016	2.020	2.010	2.042
V–O ⁴	1.933	1.940	1.941	1.953
V–O ⁵	2.016	2.020	2.024	2.001
V–OH ₂	–	–	2.103	2.095
O ¹ –V–OH ₂	–	–	92.8	99.4
O ¹ –V–O ²	112.6	108.4	161.7	166.9
O ¹ –V–O ³	101.1	103.9	99.3	92.8
O ¹ –V–O ⁴	112.6	108.2	108.8	101.8
O ¹ –V–O ⁵	101.1	104.1	97.9	103.9

O ² –V–O ⁴	134.7	88.5	89.6	86.0
O ² –V–O ⁵	86.0	147.2	82.6	86.7
O ³ –V–O ⁴	86.0	147.7	85.5	165.3
O ³ –V–O ⁵	157.9	82.9	162.7	89.3

^a Calculations performed at the B3P86/6-311g level of theory. ^b The numbering of the atoms is the same as in Figure 4. ^c Bond lengths in Å and bond angles in degrees.

3.3. V^{IV}O²⁺/levofloxacin (Hlev) system

Levofloxacin and its V^{IV}O complexes are more soluble in water than the corresponding species in the systems containing nalidixic acid and, for this reason, potentiometric titrations were performed in H₂O. The species distribution diagram as a function of pH for the system V^{IV}O²⁺/Hlev is shown in Figure 5. Using a metal to ligand molar ratio of 1:2 and V^{IV}O²⁺ concentration of 1.0 × 10^{−3} M, the major species revealed by potentiometry are [VO(HL)]²⁺, [VO(HL)₂]²⁺, [VO(HL)(L)]⁺, and [VOL₂], while the amount of [VOL]⁺ and [VOL(OH)] is very low. In [VO(HL)]²⁺ the coordination mode of the ligand is (COO[−], CO) with piperazine-NH⁺ still protonated, in [VO(HL)₂]²⁺ the coordination is 2 × (COO[−], CO) with two piperazine-NH⁺, whereas [VO(HL)(L)]⁺ and [VOL₂] are formed from [VO(HL)₂]²⁺ upon deprotonation of one and two –NH⁺ groups; p*K* of [VO(HL)₂]²⁺ are 7.20 and 7.93, comparable with 8.08 measured for the deprotonation of the piperazinium group in the free ligand (see Table 1).

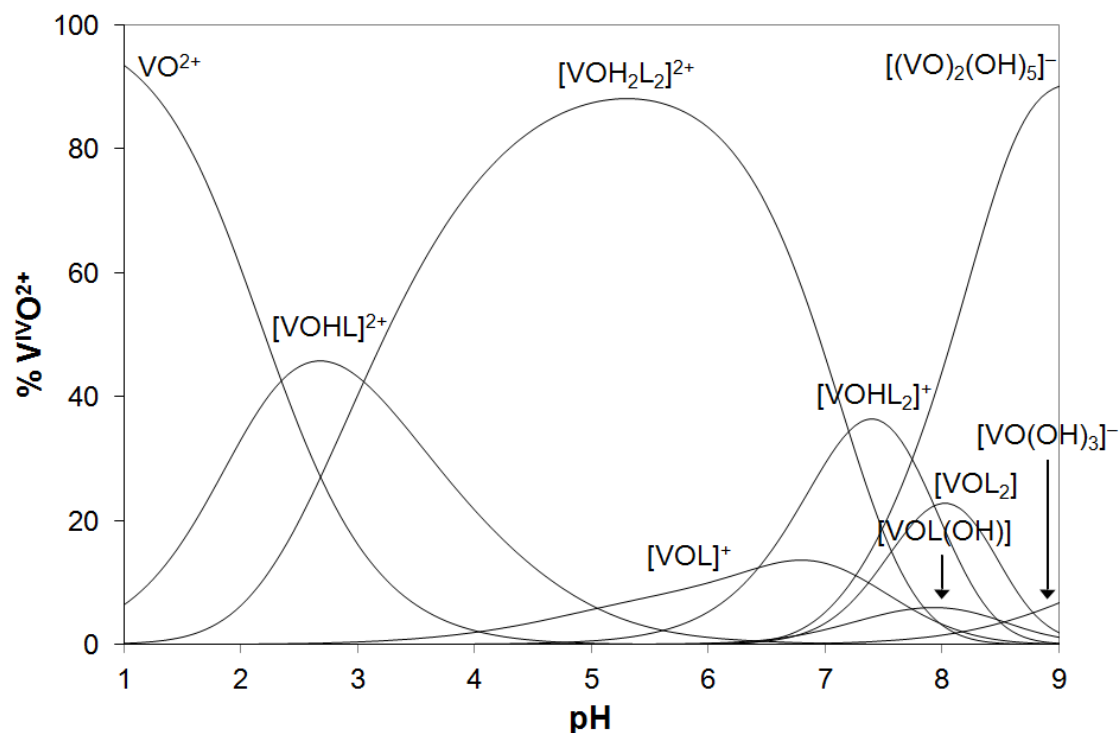


Figure 5. Distribution diagram as a function of pH of the species formed in the system $V^{IV}O^{2+}/Hlev$ (HL) with a total $V^{IV}O^{2+}$ concentration of 1.0×10^{-3} M and metal to ligand molar ratio of 1:2.

EPR spectra recorded in water in the system $V^{IV}O^{2+}/Hlev$ allowed us to confirm these results. At acidic pH values, $[VO(HL)]^{2+}$ is formed (**I** in Figure S2 of ESI), which is the major species in solution in the pH range 2-3. The value of g_z and A_z are 1.942 and $175.2 \times 10^{-4} \text{ cm}^{-1}$. In analogy with the behaviour of the system with nalidixic acid, we can suppose that the ligand binds $V^{IV}O^{2+}$ ion with the donor set (CO, COO^-) and two water molecules in the equatorial plane and another in the axial position. At higher pH, in the range 4-8, EPR signals of two species in equilibrium are detected; they were assigned to the hexa-coordinated *cis*-octahedral complex with (CO, COO^- ; CO, COO^- ; H_2O) or (CO, COO^- ; CO^{ax} , COO^- ; H_2O) coordination mode (**II** in Figure S2) and to the penta-coordinated square pyramidal one with (CO, COO^- ; CO, COO^-) coordination (**III** in Figure S2). The octahedral species is characterized by $g_z = 1.940$ and $A_z = 174.0 \times 10^{-4} \text{ cm}^{-1}$, whereas the square pyramidal complex by $g_z = 1.946$ and $A_z = 167.7 \times 10^{-4} \text{ cm}^{-1}$. These values are in line with those expected on the basis of the “additivity rule”³⁹ and DFT calculations on the $V^{IV}O$ species formed by the model ligand L^Q (Table S1 of ESI).

For comparison, EPR spectra were recorded in $H_2O/DMSO$ 50/50 (w/w), where the resolution is better than in aqueous solution (Figure S3 of ESI). The comparison between the spectra of the bis-chelated species recorded in H_2O and in the mixture $H_2O/DMSO$ (Figure S4 of ESI) indicates that

water favours the formation of *cis*-octahedral complex (**I** in Figure S4), whereas the presence of DMSO favours the square pyramidal species (**II** in Figure S4). A similar behaviour has been observed for 2-hydroxypyridine-*N*-oxide (Hhpo),^{30e} for which H₂O favours *cis*-[VO(hpo)₂(H₂O)] and DMSO [VO(hpo)₂].

3.4. V^{IV}O²⁺/ciprofloxacin (Hcip) system

The behaviour of ciprofloxacin (Hcip) has already been reported in the literature,^{67, 27} and the results can be summarized as follows. Potentiometric data indicate that it forms with V^{IV}O²⁺ the species [VO(Hcip)]²⁺, [VO(Hcip)₂]²⁺ and [VO(Hcip)(cip)]⁺. Based on EPR measurements (g_z 1.942 and A_z $173 \times 10^{-4} \text{ cm}^{-1}$) the authors have proposed for [VO(Hcip)₂]²⁺ the equatorial coordination of two carboxylate and two keto oxygens. The same authors reported preliminary results of X-ray structure determination.²⁷ The crystals of the bis-chelated complex were very unstable, decomposed during the analysis and, for this reason, atomic coordinates are not available; only a model in which vanadium is hexa-coordinated with one of the two Hcip ligands having an equatorial-axial arrangement and a water molecule in the fourth equatorial position was given. Concerning the coordination of [VO(Hcip)(cip)]⁺, the authors propose the deprotonation of the coordinated water molecule. Based on those results, it is not clear if the *cis*-octahedral coordination (with one water molecule in the fourth equatorial position) is preferred in the solid state against the square pyramidal one and which is the more stable coordination mode in aqueous solution.

The results obtained in this study show that ciprofloxacin behaves similarly to nalidixic acid and levofloxacin. Spin-Hamiltonian parameters (reported in Table 6) indicate that [VO(Hcip)(H₂O)₃]²⁺ with (CO, COO⁻; H₂O; H₂O; H₂O^{ax}) coordination is formed at low pH values. In the pH range of existence of the two bis-chelated species, [VO(Hcip)₂]²⁺ and [VO(Hcip)(cip)]⁺, the *cis*-octahedral and square pyramidal isomers – with (CO, COO⁻; CO, COO^{-ax}; H₂O) and (CO, COO⁻; CO, COO⁻) coordination mode, respectively – are in equilibrium until pH 10. The spectra as a function of pH from physiological pH to pH *ca.* 10 are shown in Figure S5 of ESI, where the *cis*-octahedral and square pyramidal species are indicated with **I** and **II**, respectively. The value of A_z for *cis*-octahedral complex, $173.2 \times 10^{-4} \text{ cm}^{-1}$ (Table 6), is comparable with that measured by Turel and co-workers for the solid compound and confirms the X-ray determination.²⁷

Table 6. Experimental spin-Hamiltonian parameters of the V^{IV}O²⁺ complexes formed by quinolone ligands.

System	Solvent	g_z	A_z ^a	Species
$V^{IV}O^{2+}/Hnal$	$H_2O/DMSO$ 50/50 (w/w)	1.941	175.4	$[VOL(H_2O)_3]^+$
		1.946	168.1	$[VOL_2]$
		1.940	174.6	$cis-VOL_2(H_2O)$
$V^{IV}O^{2+}/Hnal/MeIm$	H_2O	1.944	169.1	$cis-[VOL_2(MeIm)]$
$V^{IV}O^{2+}/Hlev$	H_2O	1.942	175.2	$[VO(HL)(H_2O)_3]^{2+}$
		1.940	174.0	$cis-[VOH_xL_2(H_2O)]^{x+}$
		1.946	167.7	$[VOH_xL_2]^{x+}$
$V^{IV}O^{2+}/Hlev/MeIm$	H_2O	1.945	168.5	$cis-[VOH_xL_2(MeIm)]^{x+}$
$V^{IV}O^{2+}/Hcip$	$H_2O/DMSO$ 50/50 (w/w)	1.940	174.9	$[VO(HL)(H_2O)_3]^{2+}$
		1.941	173.2	$cis-[VOH_xL_2(H_2O)]^{x+}$
		1.945	168.2	$[VOH_xL_2]^{x+}$
$V^{IV}O^{2+}/Hspar$	$H_2O/DMSO$ 50/50 (w/w)	1.941	174.9	$[VO(HL)(H_2O)_3]^{2+}$
		1.941	174.1	$cis-[VOH_xL_2(H_2O)]^{x+}$
		1.947	166.8	$[VOH_xL_2]^{x+}$
$V^{IV}O^{2+}/Hspar/MeIm$	H_2O	1.946	169.2	$cis-[VOH_xL_2(MeIm)]^{x+}$
$V^{IV}O^{2+}/Hnor$	$H_2O/DMSO$ 50/50 (w/w)	1.941	175.3	$[VO(HL)(H_2O)_3]^{2+}$
		1.941	173.5	$cis-[VOH_xL_2(H_2O)]^{x+}$
		1.946	167.8	$[VOH_xL_2]^{x+}$

^a All the A_z values are reported in 10^{-4} cm^{-1} .

3.5. $V^{IV}O^{2+}/sparfloxacin$ (*Hspar*) and $V^{IV}O^{2+}/norfloxacin$ (*Hnor*) systems

Sparfloxacin and norfloxacin behave similarly to the other ligands discussed in the sections 3.2.-3.4. They are little soluble in water and, for this reason, the EPR spectra were recorded in a mixture $H_2O/DMSO$ 50/50 (w/w). They form a mono-chelated species in the acidic pH range with composition $[VO(HL)(H_2O)_3]^{2+}$ and the piperazine nitrogen still protonated; the value of g_z is 1.941 and that of A_z is in the range $(174.9-175.3) \times 10^{-4} \text{ cm}^{-1}$ (Table 6). In weakly acidic solution and around neutrality, two bis-chelated species are revealed with *cis*-octahedral and square pyramidal geometry; their stoichiometry is $cis-[VOH_xL_2(H_2O)]^{x+}$ and $[VOH_xL_2]^{x+}$, with the charge $x = 0-2$ depending on the protonation degree of the ligand. The spin Hamiltonian parameters ($g_z = 1.941$ and $A_z = (173.5-174.1) \times 10^{-4} \text{ cm}^{-1}$ for $cis-[VOH_xL_2(H_2O)]^{x+}$, and $g_z = 1.946-1.947$ and $A_z = (166.8-$

$167.8) \times 10^{-4} \text{ cm}^{-1}$ for $[\text{VOH}_x\text{L}_2]^{x+}$, Table 6) are comparable with those measured in the systems with Hnal, Hlev and Hcip.

On the basis of the results listed in Table 6 and of the similar behaviour of all the five examined systems, it can be stated that the participation to the V binding of the other potential donors, such as pyridine-N of nalidixic acid, amino-NH₂ of sparfloxacin, piperazine-N or F-substituent, can be excluded.

3.6. Characterization of the solid compound $[\text{VO}(\text{nal})_2(\text{H}_2\text{O})]$

Psomas and its group synthesized V^{IV}O complexes with several quinolones such as oxolinic acid (Hoxol),³⁷ N-propyl-norfloxacin (Hpr-norf),⁸² enrofloxacin (Herx),⁸³ sparfloxacin,⁸⁴ and pipemidic acid (Hppa),⁸⁵ whereas Turel *et al.* prepared the V^{IV}O compound with ciprofloxacin.²⁷ In all the cases the stoichiometry is $[\text{VOL}_2(\text{H}_2\text{O})]$ with the ligands in their monodeprotonated form (at the carboxylic group). X-ray diffraction analysis of $[\text{VO}(\text{cip})_2(\text{H}_2\text{O})]$ and EPR spectra of the other compounds suggested that the geometry is *cis*-octahedral with a water ligand in the equatorial position, even if it is not clear if this is in *trans* to a COO⁻ or a CO group. In fact, ⁵¹V hyperfine coupling constant A_z varies from $170 \times 10^{-4} \text{ cm}^{-1}$ for $[\text{VO}(\text{pr-norf})_2(\text{H}_2\text{O})]$ and $[\text{VO}(\text{ppa})_2(\text{H}_2\text{O})]$ to $173\text{--}174 \times 10^{-4} \text{ cm}^{-1}$ for $[\text{VO}(\text{cip})_2(\text{H}_2\text{O})]$ and $[\text{VO}(\text{spar})_2(\text{H}_2\text{O})]$. This would denote a different equatorial donor set, (CO, COO⁻; CO^{ax}, COO⁻; H₂O) in the first case and (CO, COO⁻; CO, COO^{-ax}; H₂O) in the second one because the contribution of COO⁻ ($\sim 42 \times 10^{-4} \text{ cm}^{-1}$ ³⁹) is around $2 \times 10^{-4} \text{ cm}^{-1}$ lower than a CO ($\sim 44 \times 10^{-4} \text{ cm}^{-1}$ ³⁹).

In this study, $[\text{VO}(\text{nal})_2(\text{H}_2\text{O})]$ was synthesized from $\text{VOSO}_4 \cdot 3\text{H}_2\text{O}$ and Hnal with 1:2 ratio in a MeOH/H₂O solution (section 2.2). The carboxylic group undergoes deprotonation to yield the neutral complex. The solid compound has been characterized by elemental analysis and spectroscopic techniques (IR and EPR).

In the IR spectrum of nalidixic acid, the intense absorptions at $1712(\text{vs}) \text{ cm}^{-1}$ and $1617(\text{vs}) \text{ cm}^{-1}$ can be attributed to the stretching vibrations of (C=O)_{carb} and (C=O)_{ket} groups, respectively. In the spectrum of V^{IV}O complex, the band of CO shifts to $1605(\text{s}) \text{ cm}^{-1}$ and this indicates coordination of this group.⁸⁴ The value of the difference between the antisymmetric ($1636(\text{vs}) \text{ cm}^{-1}$) and symmetric stretching vibrations ($1384(\text{s}) \text{ cm}^{-1}$) of COO⁻, $\Delta = [\nu_{\text{as}}(\text{COO}) - \nu_{\text{s}}(\text{COO})] = 252 \text{ cm}^{-1}$, suggests a monodentate coordination of carboxylate.⁸⁶ The band at $3420(\text{m}) \text{ cm}^{-1}$ demonstrates the presence of water bound to the metal ion in the complex, and that at $972(\text{s}) \text{ cm}^{-1}$ is characteristic of V=O stretching of oxidovanadium(IV) complexes.⁸⁷

[VO(nal)₂(H₂O)] was dissolved in the mixtures DMSO/DMF 50/50 (w/w) or H₂O/DMSO 50/50 (w/w) and anisotropic EPR spectra were recorded to establish the geometry, the coordination mode of the ligand and possible isomerism reactions (Figure 6). In both the mixtures two sets of resonances appear, the first (**I** in Figure 6) with $g_z = 1.938\text{-}1.939$ and $A_z = (174.1\text{-}174.2) \times 10^{-4} \text{ cm}^{-1}$ and the second one (**II** in Figure 6) with $g_z = 1.944\text{-}1.945$ and $A_z = (168.4\text{-}168.7) \times 10^{-4} \text{ cm}^{-1}$. These values are comparable with those measured for *cis*-octahedral and square pyramidal isomers discussed in the previous sections. As demonstrated by DFT methods, **I** could be the isomer *OC*-6-32 or *OC*-6-34 and **II** the isomer *SPY*-5-12 or *SPY*-5-13. The two species are in equilibrium and in the hexa-coordinated complex a solvent (H₂O, DMF, DMSO) binds vanadium through O donor with its relative amount depending on the basicity of such a donor (H₂O > DMSO > DMF).

It is interesting to examine the EPR spectrum recorded on the MeOH refluxed solution obtained after the filtration of the solid compound (trace c of Figure 6). The first thing to be noticed is that the signals of *cis*-octahedral species **I** almost disappeared, suggesting that it precipitates and is filtered off from the solution: this is a further demonstration that the solid compound exists as isomers *OC*-6-32 or *OC*-6-34, according to the results in the literature.^{27, 37, 82-85} In the spectrum two species are revealed: the first (**II** in Figure 6) has $g_z = 1.943$ and $A_z = 169.8 \times 10^{-4} \text{ cm}^{-1}$ and it is the square pyramidal species, whereas the second one (**III** in Figure 6) has $g_z = 1.944$ and $A_z = 167.2 \times 10^{-4} \text{ cm}^{-1}$. As suggested by the data in Tables 3 and 4, this latter species could be the isomer *SPY*-5-13 ($A_z^{\text{calcd}} = 167.0 \times 10^{-4} \text{ cm}^{-1}$, Table 3) whose stability is comparable with that of *SPY*-5-12 ($\Delta G^{\text{tot}}_{\text{aq}} = 4.5 \text{ kJ/mol}$ at 298 K). DFT calculations indicate that $\Delta G^{\text{tot}}_{\text{aq}}$ at 337.85 K (boiling point of MeOH; remember that the solid compound [VO(nal)₂(H₂O)] was synthesized in this solvent) is 4.0 kJ/mol and this means that, for the Boltzmann distribution law the ratio between *SPY*-5-13 and *SPY*-5-12 should be 0.24, i.e. 19.4% of *SPY*-5-13 and 80.6% of *SPY*-5-12. These data are in agreement with the ratio between the resonances of **III** (*SPY*-5-13) and **II** (*SPY*-5-12) in Figure 6, and confirm that in solution the *cis*-octahedral and square pyramidal species coexist and their relative amount depends on the solvent and temperature. The fact that only the *cis*-octahedral isomer is isolated in the solid state could be related to the lower solubility of this compound in comparison with the square pyramidal isomer.

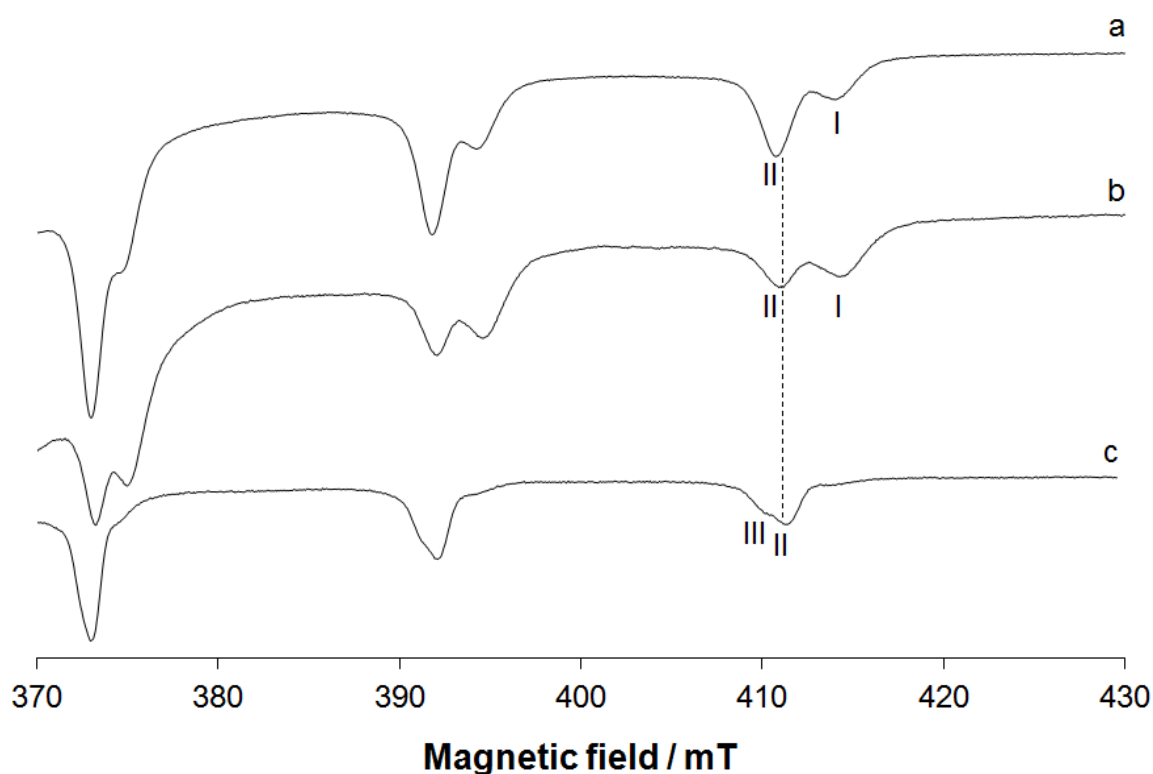


Figure 6. High field region of the X-band anisotropic EPR spectra recorded at 120 K on the solid $[\text{VO}(\text{nal})_2(\text{H}_2\text{O})]$ dissolved in a mixture DMSO/DMF 50/50 (w/w) (a), in a mixture H_2O /DMSO 50/50 (w/w) (b), and on the MeOH refluxed solution after the filtration of the solid (c). With **I**, **II** and **III** are indicated the $M_I = 7/2$ resonances of the isomers *OC*-6-32 or *OC*-6-34 (**I**), *SPY*-5-12 (**II**) and *SPY*-5-13 (**III**) of the bis-chelated species formed by nalidixic acid. The $M_I = 7/2$ resonance of *SPY*-5-12 is also denoted with the dotted line.

3.7. Interaction of the bis-chelated $\text{V}^{\text{IV}}\text{O}$ complexes with 1-methylimidazole

1-Methylimidazole (MeIm) is a good model for the coordination of a protein with an imidazole-N of a histidine residue.^{30a-h, 31b} The reason is that the protein binding to *cis*-octahedral $\text{V}^{\text{IV}}\text{O}$ complexes occurs *via* accessible histidines (often present in the protein surface) with a stabilization of secondary interactions, such as hydrogen or van der Waals contacts, which – however – do not influence the values of A_z . Therefore, the side-chain of histidine can be compared, both as structure and basicity, to a substituted imidazole.^{30b-d, 30f}

The study of the interaction of bis-chelated $\text{V}^{\text{IV}}\text{O}$ complexes with MeIm can be important because it could confirm their geometry, square pyramidal or *cis*-octahedral. In fact, only *cis*-octahedral species are able to react with MeIm upon the replacement of the weak equatorial water ligand by imidazole-N according to the equation (3):



As an example, we report here the anisotropic EPR spectra recorded in the two ternary systems $\text{V}^{\text{IV}}\text{O}^{2+}/\text{Hlev}/\text{MeIm}$ (trace b of Figure S6 of ESI) and $\text{V}^{\text{IV}}\text{O}^{2+}/\text{Hspar}/\text{MeIm}$ (trace d of Figure S6) and the comparison with the spectra measured under the same conditions in the corresponding binary systems (traces a and c of Figure S6). It can be observed that the spectra recorded in the ternary systems are different from those of the binary ones and only one species is revealed. This means that 1-methylimidazole replaces the water molecule in the *cis*-octahedral complex (indicated with **I**) to form $[\text{VO}(\text{H}_x\text{lev})_2(\text{MeIm})]^{x+}$ or $[\text{VO}(\text{H}_x\text{spar})_2(\text{MeIm})]^{x+}$ (indicated with **III**), reducing significantly the A_z value (see Table 6); the decrease of about $(4-5) \times 10^{-4} \text{ cm}^{-1}$ is in agreement with the previous results.^{30a, 30c-h} Therefore, the presence of MeIm shifts toward right the equilibrium $\text{SPY-5} + \text{H}_2\text{O} \rightleftharpoons \text{OC-6}$, subtracting progressively the octahedral species. The disappearance of the absorptions of square pyramidal complex (indicated with **II** in Figure S6) in the ternary systems confirms this finding. Analogous results were found some years ago for the system $\text{V}^{\text{IV}}\text{O}^{2+}/\text{Hdhp}$ (Hdhp is 1,2-dimethyl-3-hydroxy-4(1*H*)-pyridinone), where the formation of $[\text{VO}(\text{dhp})_2(\text{MeIm})]$ shifts the equilibrium between square pyramidal and *cis*-octahedral species toward the hexacoordinated compound.^{30a} The value of A_z for $[\text{VO}(\text{nal})_2(\text{MeIm})]$ was also predicted by DFT methods and the percent deviation, around 3%, is in agreement with what is expected (Table 3).

The results confirm that, for quinolone ligands, the species in equilibrium in aqueous or organic solution are the square pyramidal and *cis*-octahedral ones and that a protein provided with accessible donors could replace the water ligand in the equatorial plane of OC-6 isomers forming mixed species with composition $\text{VOL}_2(\text{Protein})$.

3.8. Interaction of the bis-chelated $\text{V}^{\text{IV}}\text{O}$ complexes with serum proteins

With the perspective to study the pharmacological action of V complexes of quinolones, the interaction of bis-chelated $\text{V}^{\text{IV}}\text{O}$ species with the two most important proteins devoted to the transport of the metal ions in the bloodstream – transferrin and albumin – was evaluated. In particular, the interaction of $[\text{VO}(\text{nal})_2(\text{H}_2\text{O})]$ with apo-transferrin (apo-hTf), holo-transferrin (holo-hTf) and albumin (HSA) was examined. The difference between apo-hTf and holo-hTf, as it is known, resides in the presence of two Fe^{2+} ions in the second one which affects the conformation of the protein and the recognition by the cells. In fact, the closed conformation of holo-hTf favours the receptor-mediated endocytosis and the internalization of Fe^{2+} in the cells.^{25a, 88}

EPR spectroscopy allowed many authors to obtain valuable information on the type of species formed and the amino acid residues involved in the interaction between $V^{IV}O$ complexes and proteins.³⁰⁻³¹ The EPR spectrum recorded at pH 7.4 in the ternary system $V^{IV}O^{2+}/Hnal/HSA$ is shown in trace f of Figure 7. It is characterized by one set of resonances – indicating that only one species exists in aqueous solution – with $g_z = 1.945$ and $A_z = 169.5 \times 10^{-4} \text{ cm}^{-1}$ (indicated with **VII** in Figure 7). These spin Hamiltonian parameters are similar to those detected for the ternary species *cis*-[VO(nal)₂(MeIm)] (**VI** in Figure 7) and, for this reason, the presence in solution of an analogous species formed by HSA could be supposed; for this adduct it is necessary to advance the hypothesis that a His-N donor is equatorially coordinated to $V^{IV}O^{2+}$ ion, similarly to what discussed in the literature for other systems [VOL₂]/HSA.^{30a, 30b, 30d-f, 31b, 31c} The composition of this species should be indicated with VO(nal)₂(HSA), even if the possibility of other stoichiometries, such as VO(nal)(HSA)(OH) or VO(nal)(HSA), with the contemporaneous coordination of the side-chain donors from albumin, cannot be excluded.⁷⁷ In any case, EPR spectroscopy indicate that, beyond any doubts, a mixed species is formed because the spectral resonances are different with respect to those of the binary system $V^{IV}O^{2+}/Hnal$ (where the *cis*-octahedral and square pyramidal species are in equilibrium, **III** and **V** in the trace d of Figure 7) and $V^{IV}O^{2+}/HSA$ (where a multinuclear species with composition (VO)_x(HSA) is formed,³⁸ **VIII** in the trace f of Figure 7).

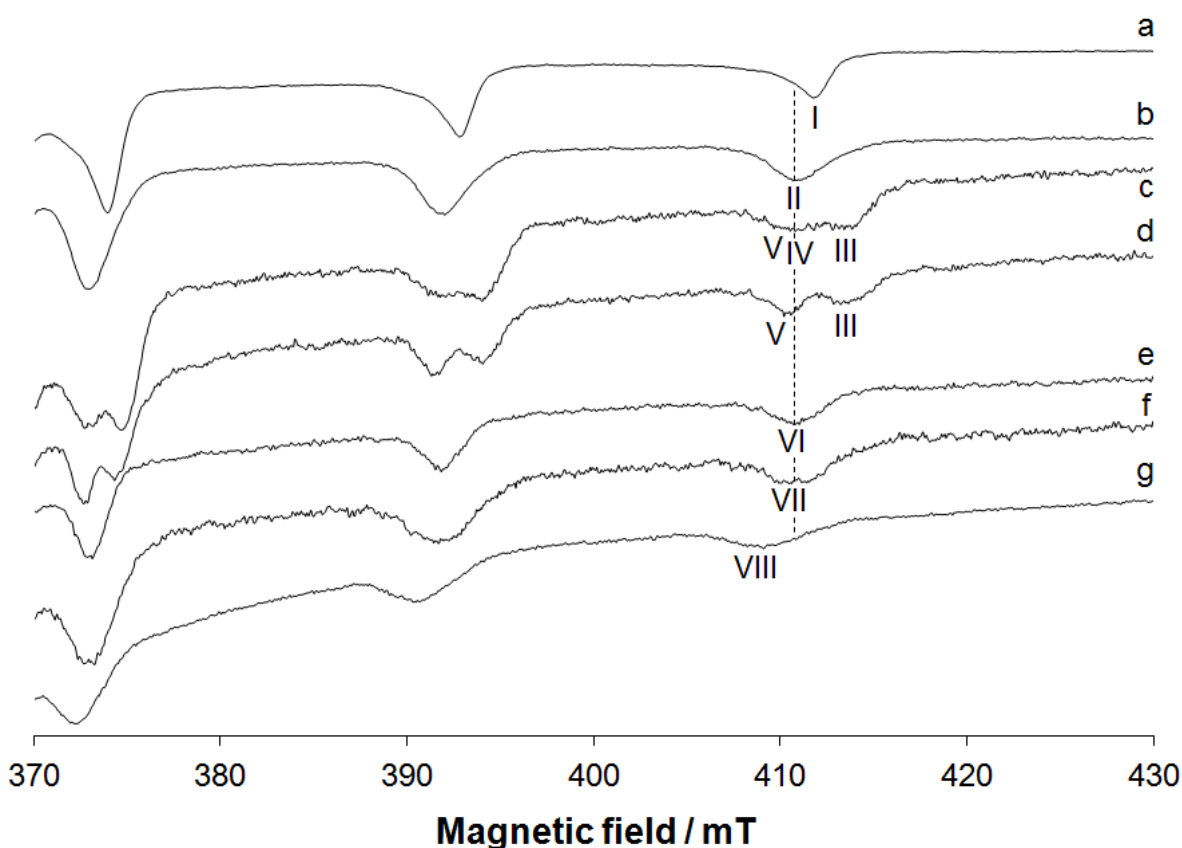


Figure 7. High field region of the X-band anisotropic EPR spectra recorded at 120 K at pH 7.4 in the system containing: a) $\text{V}^{\text{IV}}\text{O}^{2+}/\text{apo-hTf}$ 2:1 ($\text{V}^{\text{IV}}\text{O}^{2+}$ 1.0×10^{-3} M); b) $\text{V}^{\text{IV}}\text{O}^{2+}/\text{Hnal}/\text{holo-hTf}$ 2:4:1 ($\text{V}^{\text{IV}}\text{O}^{2+}$ 1.0×10^{-3} M); c) $\text{V}^{\text{IV}}\text{O}^{2+}/\text{Hnal}/\text{apo-hTf}$ 2:4:1 ($\text{V}^{\text{IV}}\text{O}^{2+}$ 1.0×10^{-3} M); d) $\text{V}^{\text{IV}}\text{O}^{2+}/\text{Hnal}$ 1:2 ($\text{V}^{\text{IV}}\text{O}^{2+}$ 1.0×10^{-3} M); e) $\text{V}^{\text{IV}}\text{O}^{2+}/\text{Hnal}/\text{MeIm}$ 1:2:4 ($\text{V}^{\text{IV}}\text{O}^{2+}$ 1.0×10^{-3} M); f) $\text{V}^{\text{IV}}\text{O}^{2+}/\text{Hnal}/\text{HSA}$ 4:8:1 ($\text{V}^{\text{IV}}\text{O}^{2+}$ 1.0×10^{-3} M) and g) $\text{V}^{\text{IV}}\text{O}^{2+}/\text{HSA}$ 4:1 ($\text{V}^{\text{IV}}\text{O}^{2+}$ 1.0×10^{-3} M). With **I**, **II**, **III**, **IV**, **V**, **VI**, **VII** and **VIII** are indicated the $M_I = 7/2$ resonances of the species $(\text{VO})(\text{apo-hTf})/(\text{VO})_2(\text{apo-hTf})$, $\{\text{cis-VO}(\text{nal})_2\}_y(\text{holo-hTf})$, $\text{cis-}[\text{VO}(\text{nal})_2(\text{H}_2\text{O})]$, $\text{cis-VO}(\text{nal})_2(\text{apo-hTf})$, $[\text{VO}(\text{nal})_2]$, $\text{cis-}[\text{VO}(\text{nal})_2(\text{MeIm})]$, $\{\text{cis-VO}(\text{nal})_2\}_y(\text{HSA})$ and $(\text{VO})_x(\text{HSA})$. The position of the $M_I = 7/2$ resonance of $\text{cis-VO}(\text{nal})_2(\text{Protein})$ is also denoted by the dotted line.

The EPR spectra recorded at pH 7.4 in the ternary systems $\text{V}^{\text{IV}}\text{O}^{2+}/\text{Hnal}/\text{apo-hTf}$ and $\text{V}^{\text{IV}}\text{O}^{2+}/\text{Hnal}/\text{holo-hTf}$ are very different (traces b and c of Figure 7). The spectra with holo-transferrin are characterized by only one set of resonances indicated with **II** ($g_z = 1.945$ and $A_z = 169.2 \times 10^{-4} \text{ cm}^{-1}$) and are very similar to those of the systems with MeIm or HSA, suggesting the equatorial coordination of a His-N which replaces the water ligand in $\text{cis-}[\text{VO}(\text{nal})_2(\text{H}_2\text{O})]$ to give $\text{cis-VO}(\text{nal})_2(\text{holo-hTf})$. This is the expected behaviour for this protein, which forms species with an analogous composition $\text{cis-VOL}_2(\text{holo-hTf})$ with maltolate (ma), picolinate (pic) and 1,2-dimethyl-

3-hydroxy-4(1*H*)-pyridinonate (dhp).^{30g} In contrast, in the spectrum with apo-hTf the major species are *cis*-[VO(nal)₂(H₂O)] and [VO(nal)₂] (**III** and **V** in Figure 7), whereas only a small amount of *cis*-VO(nal)₂(apo-hTf) – which coexists with the binary complexes – is formed (see the position of the resonance indicated with **IV** in Figure 7); the approximate spin-Hamiltonian parameters are $g_z \sim 1.945$ and $A_z = \sim 170 \times 10^{-4} \text{ cm}^{-1}$. The comparison of the systems with holo-hTf and apo-hTf indicate that the amount of the mixed complex *cis*-VO(nal)₂(apo-hTf) is much smaller than *cis*-VO(nal)₂(holo-hTf) and this would indicate that a lower number of His residues are accessible with apo-hTf than with holo-hTf. On the basis of the data in the literature, this behaviour is rather surprising because with small ligands such as picolinate, maltolate and 1,2-dimethyl-3-hydroxy-4(1*H*)-pyridinonate the formation of *cis*-VOL₂(Protein) is equally favoured with both the two forms of transferrin.^{30a, 30d, 30g} Therefore, we thought that this fact was worth being studied with other techniques.

Docking methods were recently applied to predict by blind calculations without any geometric constraints and energy restraints the X-ray structures of 39 (metal complex)–proteins with the monodentate binding of an amino acid residue to the metal ion (Mg, V, Cr, Mn, Cu, Fe, Co, Ni, Cu, Zn, Ru, Rh, Re, Os, Pt, and Au),⁶⁴ and – also – allowed us to find the binding site of the potential antidiabetic drugs [VO(pic)₂(H₂O)] and [VO(ma)₂(H₂O)] in a model protein such as lysozyme.⁶² On this basis, we optimized through DFT calculations the structures of the eight enantiomers *OC*-6 of [VO(nal)₂(H₂O)] (i.e., the Δ and Λ series of *OC*-6-34, *OC*-6-34, *OC*-6-23 and *OC*-6-24, see Scheme S3 of ESI), removed the equatorial water and blind docked the moiety *cis*-VO(nal)₂ to the structures of apo-hTf (PDB: 2hau⁵⁸), holo-hTf (3v83⁵⁹) and HSA (1ao6⁵⁷) using the parameters recently optimized for vanadium.^{62, 64} The docking assay was based on the hypothesis suggested by EPR, i.e. the monodentate coordination of a His-N donor to the moiety *cis*-VO(nal)₂. To identify the candidate residues, a relative SES (Solvent Excluded Surface) calculation was performed for the X-ray structures of apo-, holo-hTf and HSA. The results show that the potential donors are His25, His289, His349, His473, His606 and His642 for holo-hTf, while they are His25, His289, His349, His350, His606 and His642 for apo-hTf. For HSA the four residues His105, His128, His367 and His510 were considered. To ensure that the flexibility of the side chains was represented as correctly as possible, the Dunbrack rotamers libraries⁶¹ were applied during the calculations for the selected histidines and the neighbouring residues.

If apo- and holo-transferrin are taken into account, the performed dockings confirm the EPR data analysis, showing a clear coordination preference for holo-hTf. It can be noticed that the scoring values obtained (F_{max} in Table 7) are generally more than 15 GoldScore units higher than those of the apo form. In particular, for the best solution of VO(nal)₂(holo-hTf) the scoring is 68.65, in

contrast with 44.96 obtained for VO(nal)₂(apo-hTf). The lengths predicted for V^{IV}–N(His) bonds, ranging from 2.062 to 2.485 Å, are coherent with the experimental values for V^{IV}–N(imidazole) coordination.⁸⁹ Furthermore, from a statistical point of view, the holo form offers more residues able to coordinate the metal moiety than apo-hTf and binds almost all of the enantiomers of *cis*-VO(nal)₂; in contrast, apo-hTf has a unique His residue capable to bind V species, His289, and this interacts only with the isomer *OC*-6-23-Δ (see Table 7). Overall, for holo-hTf at least three His are in the correct position to coordinate *cis*-VO(nal)₂ (His25, His359 and His606), while for apo-hTf only His289 seems to be able to bind this moiety. For this reason, the adduct formed by holo-hTf can be indicated as {VO(nal)₂}_y(holo-hTf), where *y* denotes the number of *cis*-VO(nal)₂ moieties bound to His and is in the range 1-3 (depending on the ratio VO(nal)₂/holo-hTf), whereas that with apo-hTf can be denoted as VO(nal)₂(apo-hTf) because only a VO(nal)₂ moiety is bound to the polypeptide chain through His289. In Figure 8 the identified binding sites and their position in the polypeptide chain of the two forms of serum transferrin are shown.

Table 7. Docking results of the interaction of *cis*-VO(nal)₂ moiety with holo- and apo-hTf.

Residue	Isomer	$F_{\max}^{\text{a,b}}$	$F_{\text{mean}}^{\text{a,c}}$	$S_{\text{hbond}}^{\text{ext}}$ (mean) ^d	$S_{\text{vdW}}^{\text{ext}}$ (mean) ^e	Tot. Pop. ^f
holo-hTf						
His25	OC-6-23-Δ/Λ	68.65	57.86	22.67	28.87	102
	OC-6-24-Δ/Λ					
	OC-6-32-Δ/Λ					
	OC-6-34-Δ/Λ					
His349	OC-6-23-Δ/Λ	57.68	54.71	19.80	28.31	36
	OC-6-32-Δ/Λ					
His606	OC-6-23-Δ/Λ	47.01	45.59	19.59	21.83	145
	OC-6-24-Λ					
	OC-6-32-Δ/Λ					
	OC-6-34-Λ					
apo-hTf						
His289	OC-6-23-Δ	44.13	44.96	20.61	30.80	40

^a Fitness value of the GoldScore scoring function, see eq. 1. ^b The value refers to the most stable pose. ^c Mean value computed considering the scoring of the most stable poses of each isomer. ^d Contribution to the total Fitness value of the intermolecular hydrogen bonds (*hbond*). ^e Contribution

to the total Fitness value of the intermolecular van der Waals interactions (vdW). ^f Total of the solutions found in the specific binding region.

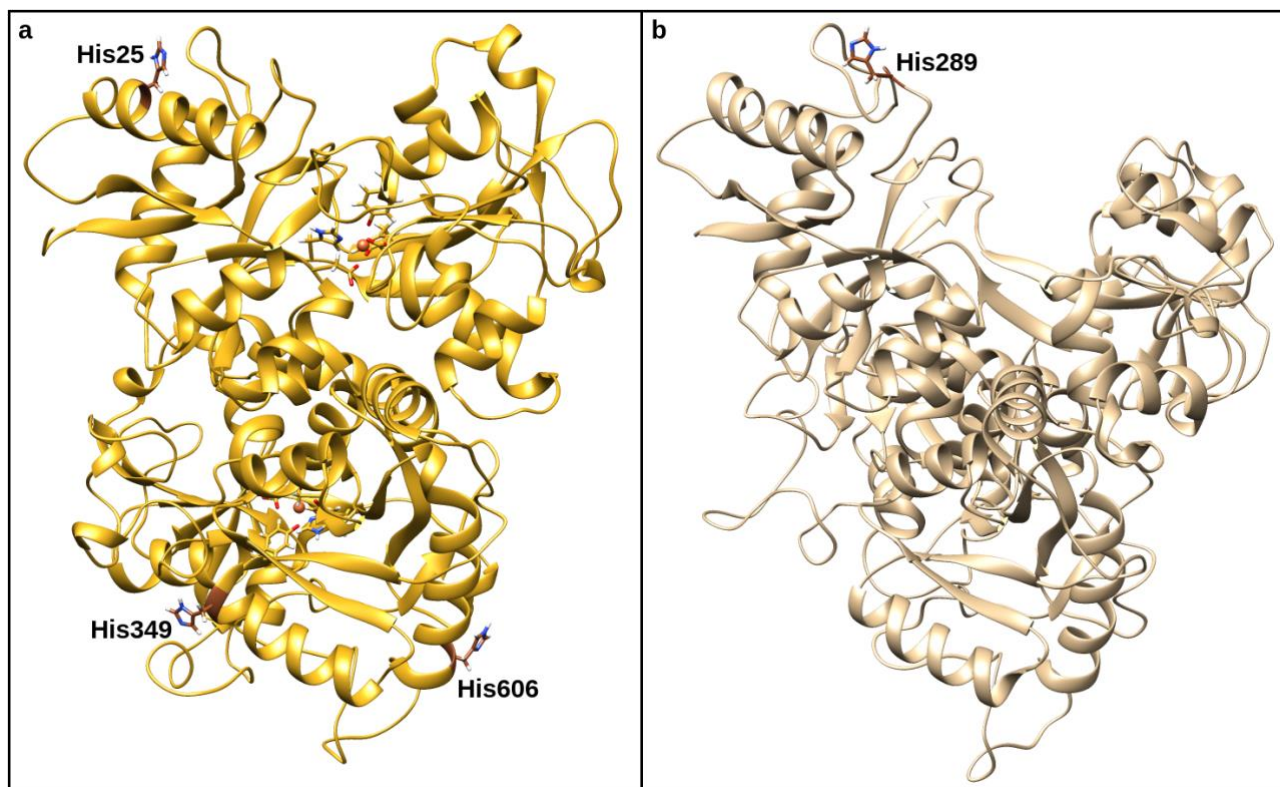


Figure 8. The histidine residues which interact more favourably with *cis*-VO(nal)₂ moiety for: a) holo-hTf and b) apo-hTf.

Looking at the energetic breakdown of the most stable poses, a QM (Quantum Mechanics) based analysis of the second coordination sphere interactions carried out with NCIPLOT (Non-Covalent Interactions Plot,⁶⁶ see section 2.8) allowed us to find a clear explanation for the different behaviour of the two principal binding sites of apo- and holo-hTf. In Figure 9 it can be observed that the number and entity of favourable strong secondary (blue blobs) and van der Waals (green blobs) interactions is the key for the different host capabilities of the two hTf folding states. In particular, the best solution *OC*-6-24- Λ -VO(nal)₂(His25-holo-hTf) presents almost five strong interactions (blue and green blobs in Figure 9) and a wide range of vdW contacts; in contrast, the solution concerning the adduct *OC*-6-23- Δ -VO(nal)₂(His289-apo-hTf) does not show significant stabilizations through strong secondary interactions, has a limited number of vdW contacts and is characterized by strong repulsive contacts (red blob in Figure 9).

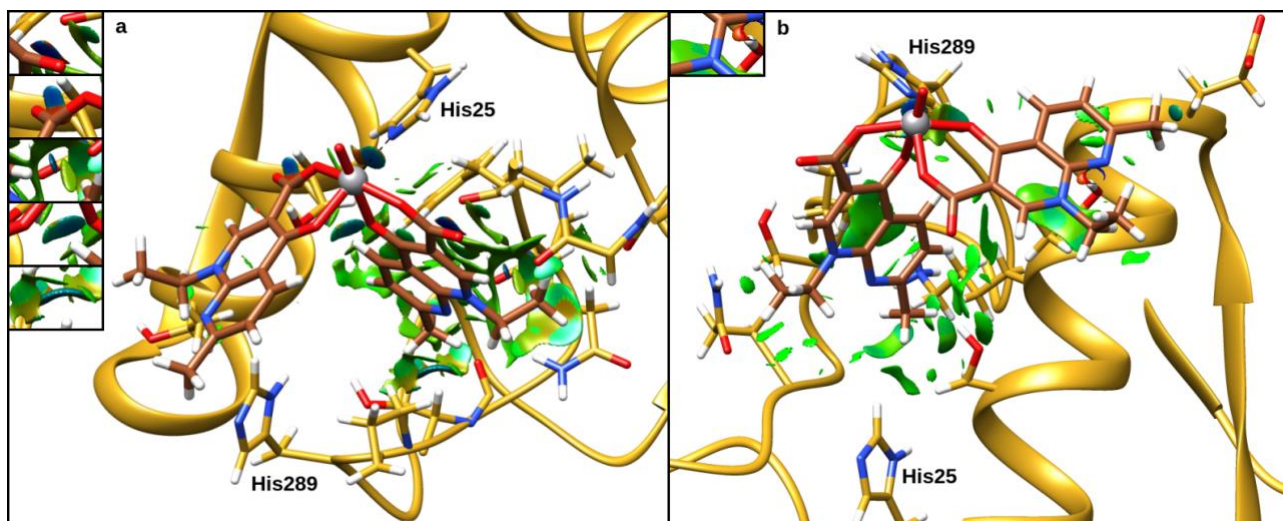


Figure 9. Gradient isosurfaces ($s = 0.3$ a.u.) analysis of the best solution of: (a) $OC-6-24-\Delta-VO(nal)_2(His25-holo-hTf)$ and (b) $OC-6-23-\Delta-VO(nal)_2(His289-apo-hTf)$. NCIPLOT surfaces show only the intermolecular interactions. The surfaces are reported in the blue-green-red scale according to values of $sign(\lambda_2) \times \rho$. Blue surfaces indicate strong attractive interactions (such as dipole-dipole or hydrogen bond), red indicates repulsions, while green means van der Waals interactions. In the insets the regions with such interactions are shown.

The simulations carried out on human serum albumin show a behaviour similar to holo-hTf, indicating at least three binding regions with high affinity for all the *cis*- $VO(nal)_2$ isomers. The most accessible histidine for $VO(nal)_2$ are His510 ($F_{max} = 61.23$), His367 ($F_{max} = 61.22$) and His105 ($F_{max} = 52.58$). In this case too, the predicted $V^{IV}-N(His)$ bond lengths are in the expected range, from 2.052 to 2.308 Å. The adduct can be described by the formula $\{VO(nal)_2\}_y(HSA)$, where $y = 1-3$ indicates that at least three *cis*- $VO(nal)_2$ moieties are bound to His residues.

On the basis of these results, the EPR spectra can be rationalized: in fact, the signals due to the adducts formed by holo-hTf and HSA (**II** and **VII** in Figure 7) are much more intense than those of the mixed species of apo-hTf (**IV** in Figure 7) and they emerge clearly with respect to the resonances of the binary $V^{IV}O$ complexes of nalidixic acid because of their higher concentration.

4. Conclusions

The family of quinolones represents one of the most commonly prescribed antibacterials in the world. Their chemical structure can allow the formation of stable complexes with transition metals,

among which vanadium, upon the formation of one or two chelated rings. The advantage of quinolones over other possible organic ligands in the developments of potential V based drugs could be the coupling of the pharmacological action of the ligands with that of vanadium, whose compounds show spermicidal, anti-HIV, antiparasitic, antiviral, antituberculosis and, above all, antidiabetic and antitumor activity. Furthermore, most of quinolones are not toxic, have already overcome the clinical tests and easily penetrate the body membranes.

In this work we have demonstrated that, at physiological pH, quinolones form stable bis-chelated $V^{IV}O$ species with (CO, COO⁻) coordination mode, for which the *cis*-octahedral and square pyramidal forms are in equilibrium. This information was obtained comparing the results obtained with pH-potentiometry with those attained with EPR spectroscopy, ESI-MS spectrometry and DFT calculations. To the best of our knowledge, this is the first time that an equilibrium between penta-coordinated square pyramidal and hexa-coordinated octahedral complexes is observed in solution for ligands forming six-membered chelated rings.

The formation of *cis*-octahedral species guarantees the possibility of first coordination sphere interactions with the serum protein, among which apo-, holo-transferrin and albumin. Such an interaction has been studied with the combined application of EPR and docking methods. Docking calculations provide very interesting results and demonstrate that, with these complexes, in contrast with what was observed until now, the three proteins do not behave in the same manner, holo-hTf and HSA having more His accessible for $V^{IV}O^{2+}$ binding than apo-hTf. This is due to the combined effect of two factors: on the one hand the steric hindrance of quinolones, higher than other ligands studied in the literature such as maltolate, picolinate or pyridinonate derivatives, and on the other the stabilization of the ternary species upon the formation of secondary electrostatic interactions depending on the structure of the ligand (for example, hydrogen, dipole-dipole or van der Waals interactions). Therefore, the steric requirements of the ligand and the nature of its substituents must be taken into account in the prediction of the interaction of $V^{IV}O$ complexes (and, in general, of metal species) with the proteins. In this specific study, the interaction of *cis*-octahedral species $[VO(nal)_2(H_2O)]$ with apo-hTf, holo-hTf and HSA results in the formation of two different species: whereas apo-hTf forms the simple $VO(nal)_2(apo-hTf)$ adduct with the coordination of His289, holo-hTf and HSA give the mixed species $\{VO(nal)_2\}_y(holo-hTf)$ and $\{VO(nal)_2\}_y(HSA)$, where $y = 1-3$ is the number of $VO(nal)_2$ moieties bound to the proteins through residues of accessible histidines (His25, His349 and His606 for holo-hTf, and His105, His367 and His510 for HSA).

The ternary species with holo-hTf, which is characterized by a closed conformation, can be recognized and internalized by the cells of the target organs in the receptor-mediated endocytosis, favouring the uptake of V based drug. This could result in a lowering of the amount/concentration

of these complexes that should be administered in a potential therapy and, therefore, in a decrease of the toxic and side-effects of the metal. This possibility could make these compounds worth being the object of future investigations in medicinal inorganic chemistry.

Conflicts of interest

There are no conflicts to declare.

Acknowledgement

This research was supported by Fondazione di Sardegna (FdS15Garribba) and European Union, and co-financed by the European Regional Development Fund under the project GINOP-2.3.2-15-2016-00008. G.S. thanks the Universitat Autònoma de Barcelona for the support to his Ph.D. grant.

References

1. M. I. Andersson and A. P. MacGowan, *J. Antimicrob. Chemother.*, 2003, **51**, 1-11.
2. A. M. Emmerson and A. M. Jones, *J. Antimicrob. Chemother.*, 2003, **51**, 13-20.
3. V. T. Andriole, *Clinical Infectious Diseases*, 2005, **41**, S113-S119.
4. L. A. Mitscher, *Chem. Rev.*, 2005, **105**, 559-592.
5. S. Heeb, M. P. Fletcher, S. R. Chhabra, S. P. Diggle, P. Williams and M. Cámara, *FEMS Microbiol. Rev.*, 2011, **35**, 247-274.
6. G. Cheng, H. Hao, M. Dai, Z. Liu and Z. Yuan, *Eur. J. Med. Chem.*, 2013, **66**, 555-562.
7. A. Dalhoff, *Infection*, 2012, **40**, 239-262.
8. K. J. Aldred, R. J. Kerns and N. Osheroff, *Biochemistry*, 2014, **53**, 1565-1574.
9. G. Y. Leshner, E. J. Froelich, M. D. Gruett, J. H. Bailey and R. P. Brundage, *J. Med. Pharm. Chem.*, 1962, **5**, 1063-1065.
10. G. E. Stein, *Pharmacotherapy*, 1988, **8**, 301-314.
11. D. E. King, R. Malone and S. H. Lillley, *Am. Fam. Physician.*, 2000, **61**, 2741-2748.
12. D. C. Hooper, *Drugs*, 1999, **58**, 6-10.
13. I. Turel, *Coord. Chem. Rev.*, 2002, **232**, 27-47.
14. V. Uivarosi, S. F. Barbuceanu, V. Aldea, C.-C. Arama, M. Badea, R. Olar and D. Marinescu, *Molecules*, 2010, **15**, 1578-1589.
15. S. Lecomte, M. H. Baron, M. T. Chenon, C. Couprie and N. J. Moreau, *Antimicrob. Agents Chemother.*, 1994, **38**, 2810-2816.
16. M. Kara, B. B. Hasinoff, D. W. McKay and N. R. Campbell, *Br. J. Clin. Pharmacol.*, 1991, **31**, 257-261.
17. K.-M. Deppermann and H. Lode, *Drugs*, 1993, **45**, 65-72.
18. G. Psomas and D. P. Kessissoglou, *Dalton Trans.*, 2013, **42**, 6252-6276.
19. (a) J. Costa Pessoa and I. Tomaz, *Curr. Med. Chem.*, 2010, **17**, 3701-3738; (b) J. Costa Pessoa, S. Etcheverry and D. Gambino, *Coord. Chem. Rev.*, 2015, **301-302**, 24-48.
20. I. E. Leon, J. F. Cadavid-Vargas, A. L. Di Virgilio and S. B. Etcheverry, *Curr. Med. Chem.*, 2017, **24**, 112-148.
21. (a) K. H. Thompson, J. H. McNeill and C. Orvig, *Chem. Rev.*, 1999, **99**, 2561-2572; (b) K. H. Thompson and C. Orvig, *Coord. Chem. Rev.*, 2001, **219-221**, 1033-1053; (c) H. Sakurai, Y. Kojima, Y. Yoshikawa, K. Kawabe and H. Yasui, *Coord. Chem. Rev.*, 2002, **226**, 187-198; (d) Y. Shechter, I. Goldwasser, M. Mironchik, M. Fridkin and D. Gefel, *Coord. Chem. Rev.*, 2003, **237**, 3-11; (e) K. Kawabe, Y. Yoshikawa, Y. Adachi and H. Sakurai, *Life Sci.*, 2006, **78**,

- 2860-2866; (f) H. Sakurai, Y. Yoshikawa and H. Yasui, *Chem. Soc. Rev.*, 2008, **37**, 2383-2392.
22. (a) V. G. Yuen, P. Caravan, L. Gelmini, N. Glover, J. H. McNeill, I. A. Setyawati, Y. Zhou and C. Orvig, *J. Inorg. Biochem.*, 1997, **68**, 109-116; (b) B. A. Reul, S. S. Amin, J.-P. Buchet, L. N. Ongemba, D. C. Crans and S. M. Brichard, *Br. J. Pharmacol.*, 1999, **126**, 467-477; (c) S. S. Amin, K. Cryer, B. Zhang, S. K. Dutta, S. S. Eaton, O. P. Anderson, S. M. Miller, B. A. Reul, S. M. Brichard and D. C. Crans, *Inorg. Chem.*, 2000, **39**, 406-416; (d) M. Rangel, A. Tamura, C. Fukushima and H. Sakurai, *J. Biol. Inorg. Chem.*, 2001, **6**, 128-132; (e) K. H. Thompson, B. D. Liboiron, Y. Sun, K. D. Bellman, I. A. Setyawati, B. O. Patrick, V. Karunaratne, G. Rawji, J. Wheeler, K. Sutton, S. Bhanot, C. Cassidy, J. H. McNeill, V. G. Yuen and C. Orvig, *J. Biol. Inorg. Chem.*, 2003, **8**, 66-74.
 23. (a) H. Sakurai, K. Fujii, S. Fujimoto, Y. Fujisawa, K. Takechi and H. Yasui, in *Vanadium Compounds: Chemistry, Biochemistry and Therapeutic Applications*, American Chemical Society, 1998, vol. 711, ch. 27, pp. 344-352; (b) H. Sakurai, Y. Fujisawa, S. Fujimoto, H. Yasui and T. Takino, *J. Trace Elem. Exp. Med.*, 1999, **12**, 393-401; (c) J. Gätjens, B. Meier, Y. Adachi, H. Sakurai and D. Rehder, *Eur. J. Inorg. Chem.*, 2006, 3575-3585; (d) H. Sakurai, in *Vanadium: The Versatile Metal*, American Chemical Society, 2007, vol. 974, ch. 9, pp. 110-120; (e) M. T. Cocco, V. Onnis, G. Ponticelli, B. Meier, D. Rehder, E. Garribba and G. Micera, *J. Inorg. Biochem.*, 2007, **101**, 19-29; (f) H. Esbak, E. A. Enyedy, T. Kiss, Y. Yoshikawa, H. Sakurai, E. Garribba and D. Rehder, *J. Inorg. Biochem.*, 2009, **103**, 590-600; (g) H. Sakurai, K. Fujii, H. Watanabe and H. Tamura, *Biochem. Biophys. Res. Commun.*, 1995, **214**, 1095-1101.
 24. (a) K. H. Thompson and C. Orvig, in *Met. Ions Biol. Syst.*, eds. H. Sigel and A. Sigel, Marcel Dekker, New York, 2004, vol. 41, pp. 221-252; (b) K. H. Thompson, B. D. Liboiron, G. R. Hanson and C. Orvig, in *Medicinal Inorganic Chemistry*, American Chemical Society, 2005, vol. 903, ch. 21, pp. 384-399; (c) K. H. Thompson and C. Orvig, *J. Inorg. Biochem.*, 2006, **100**, 1925-1935; (d) K. H. Thompson, J. Lichter, C. LeBel, M. C. Scaife, J. H. McNeill and C. Orvig, *J. Inorg. Biochem.*, 2009, **103**, 554-558.
 25. (a) D. Rehder, *Future Med. Chem.*, 2012, **4**, 1823-1837; (b) D. Rehder, *Future Med. Chem.*, 2016, **8**, 325-338.
 26. (a) E. G. Ferrer, M. V. Salinas, M. J. Correa, L. G. Naso, D. Barrio, S. B. Etcheverry, L. Lezama, T. Rojo and P. A. M. Williams, *J. Biol. Inorg. Chem.*, 2006, **11**, 791-801; (b) I. E. Leon, A. L. Di Virgilio, V. Porro, C. I. Muglia, L. G. Naso, P. A. M. Williams, M. Bollati-Fogolin and S. B. Etcheverry, *Dalton Trans.*, 2013, **42**, 11868-11880; (c) L. G. Naso, L.

- Lezama, T. Rojo, S. B. Etcheverry, M. Valcarcel, M. Roura, C. Salado, E. G. Ferrer and P. A. M. Williams, *Chem.-Biol. Interact.*, 2013, **206**, 289-301; (d) A. L. Di Virgilio, I. E. León, C. A. Franca, I. Henao, G. Tobón and S. B. Etcheverry, *Mol. Cell. Biochem.*, 2013, **376**, 53-61; (e) I. E. Leon, V. Porro, A. L. Virgilio, L. G. Naso, P. A. M. Williams, M. Bollati-Fogolín and S. B. Etcheverry, *J. Biol. Inorg. Chem.*, 2014, **19**, 59-74; (f) I. E. Leon, P. Diez, E. J. Baran, S. B. Etcheverry and M. Fuentes, *Metallomics*, 2017, **9**, 891-901.
27. I. Turel, A. Golobič, A. Klavžar, B. Pihlar, P. Buglyó, E. Tolis, D. Rehder and K. Sepčić, *J. Inorg. Biochem.*, 2003, **95**, 199-207.
28. D. Rehder, in *Interrelations between Essential Metal Ions and Human Diseases*, eds. A. Sigel, H. Sigel and R. K. O. Sigel, Springer Science+Business Media, Dordrecht, 2013, ch. 5, pp. 139-169.
29. J. Costa Pessoa, E. Garribba, M. F. A. Santos and T. Santos-Silva, *Coord. Chem. Rev.*, 2015, **301-302**, 49-86.
30. (a) D. Sanna, G. Micera and E. Garribba, *Inorg. Chem.*, 2010, **49**, 174-187; (b) D. Sanna, P. Buglyó, G. Micera and E. Garribba, *J. Biol. Inorg. Chem.*, 2010, **15**, 825-839; (c) D. Sanna, G. Micera and E. Garribba, *Inorg. Chem.*, 2011, **50**, 3717-3728; (d) D. Sanna, L. Biro, P. Buglyo, G. Micera and E. Garribba, *Metallomics*, 2012, **4**, 33-36; (e) D. Sanna, V. Ugone, G. Micera and E. Garribba, *Dalton Trans.*, 2012, **41**, 7304-7318; (f) D. Sanna, L. Bíró, P. Buglyó, G. Micera and E. Garribba, *J. Inorg. Biochem.*, 2012, **115**, 87-99; (g) D. Sanna, G. Micera and E. Garribba, *Inorg. Chem.*, 2013, **52**, 11975-11985; (h) D. Sanna, M. Serra, G. Micera and E. Garribba, *Inorg. Chem.*, 2014, **53**, 1449-1464; (i) D. Sanna, M. Serra, G. Micera and E. Garribba, *Inorg. Chim. Acta*, 2014, **420**, 75-84; (j) D. Sanna, V. Ugone, L. Pisano, M. Serra, G. Micera and E. Garribba, *J. Inorg. Biochem.*, 2015, **153**, 167-177; (k) T. Koleša-Dobravc, E. Lodyga-Chruscinska, M. Symonowicz, D. Sanna, A. Meden, F. Perdih and E. Garribba, *Inorg. Chem.*, 2014, **53**, 7960-7976; (l) D. Sanna, V. Ugone, G. Micera, T. Pivetta, E. Valletta and E. Garribba, *Inorg. Chem.*, 2015, **54**, 8237-8250.
31. (a) G. R. Willsky, A. B. Goldfine, P. J. Kostyniak, J. H. McNeill, L. Q. Yang, H. R. Khan and D. C. Crans, *J. Inorg. Biochem.*, 2001, **85**, 33-42; (b) B. D. Liboiron, K. H. Thompson, G. R. Hanson, E. Lam, N. Aebischer and C. Orvig, *J. Am. Chem. Soc.*, 2005, **127**, 5104-5115; (c) B. D. Liboiron, in *High Resolution EPR*, eds. L. Berliner and G. Hanson, Springer New York, 2009, vol. 28, ch. 12, pp. 507-549; (d) T. Jakusch, D. Hollender, E. A. Enyedy, C. S. Gonzalez, M. Montes-Bayon, A. Sanz-Medel, J. Costa Pessoa, I. Tomaz and T. Kiss, *Dalton Trans.*, 2009, 2428-2437; (e) I. Correia, T. Jakusch, E. Cobbinna, S. Mehtab, I. Tomaz, N. V. Nagy, A. Rockenbauer, J. Costa Pessoa and T. Kiss, *Dalton Trans.*, 2012, **41**, 6477-6487; (f)

- S. Mehtab, G. Gonçalves, S. Roy, A. I. Tomaz, T. Santos-Silva, M. F. A. Santos, M. J. Romão, T. Jakusch, T. Kiss and J. Costa Pessoa, *J. Inorg. Biochem.*, 2013, **121**, 187-195; (g) G. Gonçalves, A. I. Tomaz, I. Correia, L. F. Veiros, M. M. C. A. Castro, F. Avecilla, L. Palacio, M. Maestro, T. Kiss, T. Jakusch, M. H. V. Garcia and J. Costa Pessoa, *Dalton Trans.*, 2013, **42**, 11841-11861; (h) M. F. A. Santos, I. Correia, A. R. Oliveira, E. Garribba, J. Costa Pessoa and T. Santos-Silva, *Eur. J. Inorg. Chem.*, 2014, 3293-3297.
32. Y. Yoshikawa, H. Sakurai, D. C. Crans, G. Micera and E. Garribba, *Dalton Trans.*, 2014, **43**, 6965-6972.
 33. G. Micera and D. Sanna, in *Vanadium in the environment Part I: Chemistry and Biochemistry*, ed. J. O. Nriagu, Wiley, New York, 1998, pp. 131-166.
 34. S. M. Meier, C. Gerner, B. K. Keppler, M. A. Cinellu and A. Casini, *Inorg. Chem.*, 2016, **55**, 4248-4259.
 35. F. Neese, *Coord. Chem. Rev.*, 2009, **253**, 526-563.
 36. I. Nagypál and I. Fábián, *Inorg. Chim. Acta*, 1982, **61**, 109-113.
 37. A. Tarushi, P. Christofis and G. Psomas, *Polyhedron*, 2007, **26**, 3963-3972.
 38. (a) D. Sanna, E. Garribba and G. Micera, *J. Inorg. Biochem.*, 2009, **103**, 648-655; (b) D. Sanna, G. Micera and E. Garribba, *Inorg. Chem.*, 2009, **48**, 5747-5757.
 39. (a) D. N. Chasteen, in *Biological Magnetic Resonance*, eds. L. J. J. Berliner and J. Reuben, Plenum Press, New York, 1981, vol. 3, ch. 2, pp. 53-119; (b) T. S. Smith II, R. LoBrutto and V. L. Pecoraro, *Coord. Chem. Rev.*, 2002, **228**, 1-18; (c) E. Garribba, E. Lodyga-Chruscinska, G. Micera, A. Panzanelli and D. Sanna, *Eur. J. Inorg. Chem.*, 2005, 1369-1382.
 40. T. Mussini, A. K. Covington, P. Longhi and S. Rondinini, *Pure Appl. Chem.*, 1985, **57**, 865-876.
 41. H. M. Irving, M. G. Miles and L. D. Pettit, *Anal. Chim. Acta*, 1967, **38**, 475-488.
 42. D. M. Griffith, B. Szöcs, T. Keogh, K. Y. Suponitsky, E. Farkas, P. Buglyó and C. J. Marmion, *J. Inorg. Biochem.*, 2011, **105**, 763-769.
 43. L. Zékány and I. Nagypál, in *Computation Methods for the Determination of Formation Constants*, ed. D. J. Leggett, Plenum Press, New York, 1985, pp. 291-353.
 44. R. P. Henry, P. C. H. Mitchell and J. E. Prue, *J. Chem. Soc., Dalton Trans.*, 1973, 1156-1159.
 45. C. W. Davies, *J. Chem. Soc.*, 1938, 2093-2098.
 46. A. Komura, M. Hayashi and H. Imanaga, *Bull. Chem. Soc. Jpn.*, 1977, **50**, 2927-2931.
 47. L. F. Vilas Boas and J. Costa Pessoa, in *Comprehensive Coordination Chemistry*, eds. G. Wilkinson, R. D. Gillard and J. A. McCleverty, Pergamon Press, Oxford, 1985, vol. 3, pp. 453-583.

48. M. J. Frisch, G. W. Trucks, H. B. Schlegel, G. E. Scuseria, M. A. Robb, J. R. Cheeseman, G. Scalmani, V. Barone, B. Mennucci, G. A. Petersson, H. Nakatsuji, M. L. Caricato, X., H. P. Hratchian, A. F. Izmaylov, J. Bloino, G. Zheng, J. L. Sonnenberg, M. Hada, M. Ehara, K. Toyota, R. Fukuda, J. Hasegawa, M. Ishida, T. Nakajima, Y. Honda, O. Kitao, H. Nakai, T. Vreven, J. A. Montgomery, Jr., J. E. Peralta, F. Ogliaro, M. Bearpark, J. J. Heyd, E. Brothers, K. N. Kudin, V. N. Staroverov, T. Keith, R. Kobayashi, J. Normand, K. Raghavachari, A. Rendell, J. C. Burant, S. S. Iyengar, J. Tomasi, M. Cossi, N. Rega, J. M. Millam, M. Klene, J. E. Knox, J. B. Cross, V. Bakken, C. J. Adamo, J., R. Gomperts, R. E. Stratmann, O. Yazyev, A. J. Austin, R. Cammi, C. Pomelli, J. W. Ochterski, R. L. Martin, K. Morokuma, V. G. Zakrzewski, G. A. Voth, P. Salvador, J. J. Dannenberg, S. Dapprich, A. D. Daniels, Ö. Farkas, J. B. Foresman, J. V. Ortiz, J. Cioslowski and D. J. Fox, *Gaussian 09, revision C.01*, Gaussian, Inc., Wallingford, CT, 2010.
49. G. Micera and E. Garribba, *Int. J. Quantum Chem.*, 2012, **112**, 2486-2498.
50. (a) M. Bühl and H. Kabrede, *J. Chem. Theory Comput.*, 2006, **2**, 1282-1290; (b) M. Bühl, C. Reimann, D. A. Pantazis, T. Bredow and F. Neese, *J. Chem. Theory Comput.*, 2008, **4**, 1449-1459.
51. *Nomenclature of Inorganic Chemistry – IUPAC Recommendations*, Connelly, N. G.; Damhus, T.; Hartshorn, R. M.; Hutton, A. T. Eds. The Royal Society of Chemistry: Cambridge, 2005. According to IUPAC, the configuration index of square pyramidal (*SPY-5*) and octahedral (*OC-6*) complexes consists of two digits. For *SPY-5* the first digit is the priority number of the donor on the C₄ symmetry axis of the idealized pyramid and the second digit is the priority number of the donor *trans* to that with the lowest priority number in the plane perpendicular to the C₄ axis (if there is more than one of the highest priority ligand in the plane, the priority number of the *trans* ligand having the largest numerical value is selected). For *OC-6* the first digit is the priority number of the ligating atom *trans* to the ligating atom of priority number 1, and the second digit of the configuration index is the priority number of the ligating atom *trans* to the most preferred ligand in the plane that is perpendicular to the reference axis. The procedure for assigning priority numbers to the donor atoms is based upon the standard sequence rules developed for chiral carbon compounds by Cahn, Ingold and Prelog (CIP rules).
52. (a) G. Micera, V. L. Pecoraro and E. Garribba, *Inorg. Chem.*, 2009, **48**, 5790-5796; (b) G. Micera and E. Garribba, *Eur. J. Inorg. Chem.*, 2010, 4697-4710; (c) D. Sanna, K. Varnágy, S. Timári, G. Micera and E. Garribba, *Inorg. Chem.*, 2011, **50**, 10328-10341; (d) G. Micera and E. Garribba, *Eur. J. Inorg. Chem.*, 2011, 3768-3780; (e) D. Sanna, V. Pecoraro, G. Micera and

- E. Garribba, *J. Biol. Inorg. Chem.*, 2012, **17**, 773-790; (f) G. C. Justino, E. Garribba and J. Costa Pessoa, *J. Biol. Inorg. Chem.*, 2013, **18**, 803-813; (g) S. Kundu, D. Mondal, K. Bhattacharya, A. Endo, D. Sanna, E. Garribba and M. Chaudhury, *Inorg. Chem.*, 2015, **54**, 6203-6215; (h) S. P. Dash, S. Majumder, A. Banerjee, M. F. N. N. Carvalho, P. Adão, J. C. Pessoa, K. Brzezinski, E. Garribba, H. Reuter and R. Dinda, *Inorg. Chem.*, 2016, **55**, 1165-1182.
53. (a) G. Micera and E. Garribba, *Dalton Trans.*, 2009, 1914-1918; (b) G. Micera and E. Garribba, *J. Comput. Chem.*, 2011, **32**, 2822-2835; (c) D. Sanna, G. Sciortino, V. Ugone, G. Micera and E. Garribba, *Inorg. Chem.*, 2016, **55**, 7373-7387.
 54. A. V. Marenich, C. J. Cramer and D. G. Truhlar, *J. Phys. Chem. B*, 2009, **113**, 6378-6396.
 55. (a) E. Lodyga-Chruscinska, G. Micera and E. Garribba, *Inorg. Chem.*, 2011, **50**, 883-899; (b) D. Sanna, P. Buglyó, L. Bíró, G. Micera and E. Garribba, *Eur. J. Inorg. Chem.*, 2012, 1079-1092; (c) D. Sanna, P. Buglyo, A. I. Tomaz, J. Costa Pessoa, S. Borovic, G. Micera and E. Garribba, *Dalton Trans.*, 2012, **41**, 12824-12838; (d) L. Pisano, K. Varnagy, S. Timari, K. Hegetschweiler, G. Micera and E. Garribba, *Inorg. Chem.*, 2013, **52**, 5260-5272; (e) D. Sanna, K. Várnagy, N. Lihi, G. Micera and E. Garribba, *Inorg. Chem.*, 2013, **52**, 8202-8213; (f) E. Lodyga-Chruscinska, A. Szebesczyk, D. Sanna, K. Hegetschweiler, G. Micera and E. Garribba, *Dalton Trans.*, 2013, **42**, 13404-13416.
 56. G. Jones, P. Willett, R. C. Glen, A. R. Leach and R. Taylor, *J. Mol. Biol.*, 1997, **267**, 727-748.
 57. S. Sugio, A. Kashima, S. Mochizuki, M. Noda and K. Kobayashi, *Protein Eng., Des. Sel.*, 1999, **12**, 439-446.
 58. J. Wally, P. J. Halbrooks, C. Vonnrhein, M. A. Rould, S. J. Everse, A. B. Mason and S. K. Buchanan, *J. Biol. Chem.*, 2006, **281**, 24934-24944.
 59. N. Noinaj, N. C. Easley, M. Oke, N. Mizuno, J. Gumbart, E. Boura, A. N. Steere, O. Zak, P. Aisen, E. Tajkhorshid, R. W. Evans, A. R. Gorringer, A. B. Mason, A. C. Steven and S. K. Buchanan, *Nature*, 2012, **483**, 53-58.
 60. E. F. Pettersen, T. D. Goddard, C. C. Huang, G. S. Couch, D. M. Greenblatt, E. C. Meng and T. E. Ferrin, *J. Comput. Chem.*, 2004, **25**, 1605-1612.
 61. R. L. Dunbrack and M. Karplus, *J. Mol. Biol.*, 1993, **230**, 543-574.
 62. G. Sciortino, D. Sanna, V. Ugone, G. Micera, A. Lledós, J.-D. Maréchal and E. Garribba, *Inorg. Chem.*, 2017, **56**, 12938-12951.
 63. (a) C. M. L., *J. Appl. Cryst.*, 1983, **16**, 548-558; (b) C. J. Bendell, S. Liu, T. Aumentado-Armstrong, B. Istrate, P. T. Cernek, S. Khan, S. Picioreanu, M. Zhao and R. A. Murgita, *BMC Bioinformatics*, 2014, **15**, 82.

64. G. Sciortino, J. Rodríguez-Guerra Pedregal, A. Lledós, E. Garribba and J.-D. Maréchal, *J. Comput. Chem.*, 2018, **39**, 42-51.
65. (a) J. Rodríguez-Guerra, *Insilichem/gauidiview: Pre-alpha public releas*, Zenodo, 2017; (b) J. Rodríguez-Guerra Pedregal, G. Sciortino, J. Guasp, M. Municoy and J.-D. Maréchal, *J. Comput. Chem.*, 2017, **38**, 2118-2126.
66. (a) J. Contreras-García, E. R. Johnson, S. Keinan, R. Chaudret, J.-P. Piquemal, D. N. Beratan and W. Yang, *J. Chem. Theory Comput.*, 2011, **7**, 625-632; (b) R. Chaudret, B. de Courcy, J. Contreras-Garcia, E. Gloaguen, A. Zehnacker-Rentien, M. Mons and J. P. Piquemal, *Phys. Chem. Chem. Phys.*, 2014, **16**, 9876-9891.
67. I. Turel, N. Bukovec and E. Farkas, *Polyhedron*, 1996, **15**, 269-275.
68. V. Uivarosi, *Molecules*, 2013, **18**, 11153.
69. (a) M. Nakano, M. Yamamoto and T. Arita, *Chem. Pharm. Bull.*, 1978, **26**, 1505-1510; (b) A. Cole, J. Goodfield, D. R. Williams and J. M. Midgley, *Inorg. Chim. Acta*, 1984, **92**, 91-97; (c) K. Takács-Novák, B. Noszál, I. Hermecz, G. Keresztúri, B. Podányi and G. Szász, *J. Pharm. Sci.*, 1990, **79**, 1023-1028.
70. (a) A. Avdeef, *Absorption and Drug Development: Solubility, Permeability, and Charge State, Second Edition*, John Wiley & Sons, Inc, Hoboken, New Jersey, 2012; (b) A. Avdeef, *Curr. Top. Med. Chem.*, 2001, **1**, 277-351.
71. G. R. Hanson, Y. Sun and C. Orvig, *Inorg. Chem.*, 1996, **35**, 6507-6512.
72. M. Rangel, A. Leite, M. João Amorim, E. Garribba, G. Micera and E. Lodyga-Chruscinska, *Inorg. Chem.*, 2006, **45**, 8086-8097.
73. D. C. Crans, H. Chen, O. P. Anderson and M. M. Miller, *J. Am. Chem. Soc.*, 1993, **115**, 6769-6776.
74. (a) O. Bortolini, V. Conte, F. Di Furia and S. Moro, *Eur. J. Inorg. Chem.*, 1998, 1193-1197; (b) O. Bortolini, M. Carraro, V. Conte and S. Moro, *Eur. J. Inorg. Chem.*, 1999, 1489-1495; (c) M. Bonchio, O. Bortolini, V. Conte and S. Moro, *Eur. J. Inorg. Chem.*, 2001, 2913-2919; (d) O. Bortolini and V. Conte, *Mass Spectrom. Rev.*, 2006, **25**, 724-740.
75. V. B. Di Marco and G. G. Bombi, *Mass Spectrom. Rev.*, 2006, **25**, 347-379.
76. L. E. Sojo, N. Chahal and B. O. Keller, *Rapid Commun. Mass Spectrom.*, 2014, **28**, 2181-2190.
77. D. Sanna, V. Ugone, G. Micera, P. Buglyo, L. Biro and E. Garribba, *Dalton Trans.*, 2017, **46**, 8950-8967.
78. F. Belaj, A. Basch and U. Muster, *Acta Crystallogr. Sect. C*, 2000, **56**, 921-922.
79. S. Gorelsky, G. Micera and E. Garribba, *Chem.–Eur. J.*, 2010, **16**, 8167-8180.

80. A. W. Addison, T. N. Rao, J. Reedijk, J. van Rijn and G. C. Verschoor, *J. Chem. Soc., Dalton Trans.*, 1984, 1349-1356.
81. E. Lodyga-Chruscinska, D. Sanna, E. Garribba and G. Micera, *Dalton Trans.*, 2008, 4903-4916.
82. E. K. Efthimiadou, G. Psomas, Y. Sanakis, N. Katsaros and A. Karaliota, *J. Inorg. Biochem.*, 2007, **101**, 525-535.
83. E. K. Efthimiadou, N. Katsaros, A. Karaliota and G. Psomas, *Bioorg. Med. Chem. Lett.*, 2007, **17**, 1238-1242.
84. E. K. Efthimiadou, A. Karaliota and G. Psomas, *J. Inorg. Biochem.*, 2010, **104**, 455-466.
85. E. K. Efthimiadou, Y. Sanakis, N. Katsaros, A. Karaliota and G. Psomas, *Polyhedron*, 2007, **26**, 1148-1158.
86. K. Nakamoto, *Infrared and Raman Spectra of Inorganic and Coordination Compounds, fourth edition*, Wiley, New York, 1986.
87. (a) J. Selbin, *Chem. Rev.*, 1965, **65**, 153-175; (b) J. Selbin, *Coord. Chem. Rev.*, 1966, **1**, 293-314.
88. R. Crichton, *Iron Metabolism - From Molecular Mechanisms to Clinical Consequences, 3rd Edition*, John Wiley & Sons, Ltd, Chichester, 2009.
89. T. S. Smith II, C. A. Root, J. W. Kampf, P. G. Rasmussen and V. L. Pecoraro, *J. Am. Chem. Soc.*, 2000, **122**, 767-775.

Contents Entry

Text

$V^{IV}O$ complexes of quinolone derivatives (L) were studied with the aim to couple the pharmacological activity of these ligands with that of vanadium. An equilibrium between VOL_2 and $cis-VOL_2(H_2O)$ is observed at physiological pH. The interaction of $cis-VOL_2(H_2O)$, with the serum proteins indicates that the mixed species $\{VOL_2\}_y(Protein)$ are formed upon the binding of accessible histidines, with $y = 1$ for apo-hTf and $y = 1-3$ for holo-hTf and HSA.

Color graphic

